RESEARCH

Comparison and integration of simulation models for horizontal connection pipes in geothermal bore fields

Stephan Düber[1,2]* , Raul Fuentes[1] and Guillermo A. Narsilio[2]

*Correspondence:
dueber@gut.rwth-aachen.de

[1] Institute of Geomechanics & Underground Technology, RWTH Aachen University, Aachen, Germany
[2] Department of Infrastructure Engineering, The University of Melbourne, Parkville, Australia

Abstract

The heat transfer along horizontal connection pipes in geothermal bore fields can have significant effects and should not be neglected. As practical and design-related applications require simple and efficient models, we investigate suitability of different models for the first time within this context. Three ground and three pipe models of different complexity are studied. All model combinations are coupled with a fixed ground load boundary condition on one side and a borehole heat exchanger (BHE) model on the other side. Models are tested under a variety of realistic conditions to evaluate performance. The investigations show that all investigated pipe models are equally suitable for the application. For the ground models, the horizontal finite line source model and the numerical 2D model produce identical results for homogeneous ground properties. The soil resistance model neglects the temperature accumulation in the ground and thus leads to considerable deviations and should be avoided. Based on the findings, we propose a computationally efficient approach using a novel combination of established simple steady-state models for the BHE and connection pipes. In the selected example scenario, the consideration of a 30 m connection pipe attached to the BHE leads to an increase in the BHE load by 40% for the heating case and a reduction in the BHE load by 5% for the cooling case.

Keywords: Borehole heat exchanger, Horizontal connection pipe, Model comparison

Introduction

The exploitation of geothermal energy is becoming increasingly important in the context of global warming and the reduction of greenhouse gas emissions. Vertical borehole heat exchangers (BHE) or horizontal geothermal collectors using a ground source heat pump (GSHP) are the main installations to heat and cool buildings. In densely populated areas, BHEs are often preferred as they require much smaller footprint than horizontal systems. For the supply of commercial buildings, apartment blocks, or entire districts, systems with several dozen or even hundreds of BHEs are increasingly being installed. For example, in Sweden alone the number of registered installations with 10,000m or more total borehole length has almost quadrupled from 21 in 2015, to 76 systems in 2019, while the number of installations with 10 boreholes or more has increased by almost

40% during the same period Lund and Toth (2021). To reduce thermal interference between the boreholes, a minimum spacing should be maintained between the BHEs in a bore field Kavanaugh and Rafferty (2014); Energietechnik (2019). This can result in distances of several dozen meters between the BHEs and the heat pump, manifolds or header pipes. The hydraulic effects of these connection pipe networks have been investigated recently in various studies; however, without in depth consideration of their thermal interference with the surrounding ground Chen et al. (2020); Zhang et al. (2021); Chen et al. (2021). Luo et al. Luo et al. (2013) use a three-dimensional numerical model to investigate the heat loss along a single buried pipe at different depths, reporting double-digit kW h daily heat losses depending on burial depth for an 18m connection pipe. Tian et al. Tian et al. (2022) investigate the impact of burial depth, surface temperature, backfill material and flow rate on the heat loss of horizontal connection pipes connected to BHE in a sandbox experiment. In this work, the inlet temperature is fixed, leading to heat gains along the connection pipes for all investigated scenarios. For practical applications in the design and optimisation of geothermal bore fields, however, simpler and more efficient approaches are desirable. While numerical 3D models can accurately represent all types of heat transport and boundary conditions, some difficulties arise in the context borehole heat exchangers and horizontal connection pipes. Namely, the scale-distributed time ranges (hourly thermal loads and design periods of multiple decades) and geometries (pipe diameters of a few centimetres and BHE lengths of several 100 meters) lead to high modelling and computational efforts Li et al. (2014).

Heat transfer in the near-surface ground from a combination of linear or cylindrical heat sources and sinks has been investigated in various contexts over the last century. These include buried power cables, oil or steam pipelines, pipelines for district heating networks and, increasingly in recent decades, horizontal geothermal collectors. Considering the pipe diameters and fluid temperatures, the latter are most closely related to the connection pipes investigated in this work.

Several authors have derived analytical equations for the problem of heat conduction in a semi-infinite space. While Ioffe Ioffe (1972) provides a solution for transient heat conduction due to a cylinder with a fixed temperature, Thiyagarajan and Yovanovich Thiyagarajan and Yovanovich (1974) and Martin and Sadhal Martin and Sadhal (1978) provide solutions for a heat flux boundary condition at the cylinder for transient and steady state. To account for groundwater flow around the cylinder, the analytical steady-state solution of Himasekhar and Bau Himasekhar and Bau (1987) can be applied. While the boundary condition at the ground surface is a fixed temperature for the above solutions, Chung et al. Chung et al. (1999) present a semi-analytical model for a buried pipe with a constant wall temperature and a convection boundary condition at the ground surface. Including the domain inside the pipe, Hastaoglu et al. Hastaoglu et al. (1995) propose a 3D numerical model to solve the heat transfer from a buried pipe with laminar flow and solidification of the fluid. While the works mentioned so far are formulated for single pipes, Shafagh et al. Shafagh et al. (2022) consider multiple pipes in their investigation using a 2D numerical model for the domain outside the pipes.

An early, and well-known, reference on horizontal geothermal collectors is the work of Claesson and Dunand (1983). Comprehensive reviews on more recent work can be found in Hou et al. (2022); Cui et al. (2019). Similar to simulation models for borehole

heat exchangers, the spatial domain for horizontal collector models is often divided into two areas: the heat exchanger (the pipe), and the media (surrounding ground). By doing so, specifically suited calculation models for both areas can be used to reduce the computational cost. If the ground is homogeneous and heat is only transferred through conduction, analytical solutions such as the infinite or finite line source (FLS) Claesson and Dunand (1983); Fontaine et al. (2011); Lamarche (2019); Urresta et al. (2021) or ring source Li et al. (2012); Xiong et al. (2015) can be used. Spatial and temporal superposition is applied in these models to account for multiple pipes and time-dependent thermal loads Carslaw and Jaeger (1959). As the horizontal pipes are buried at shallow depths, there are situations, where transfer mechanisms other than conduction might need to be considered. Piechowski Piechowski (1999), for example, uses a 2D numerical ground model to account for moisture transport in the vicinity of the pipe. Another influencing factor can be the boundary condition at the surface above the pipes. Several authors consider evaporation, radiation and convection in their numerical 2D models Bortoloni et al. (2017); Kayaci and Demir (2018); Gan (2019); Larwa and Kupiec (2020). The models neglect temperature changes in the ground along the pipe axis, as it is negligible in most cases Claesson and Dunand (1983). Nevertheless, there are also some works in which the ground is modelled as three-dimensional, for example, to investigate different pipe arrangements Wu et al. (2010); Dasare and Saha (2015); Selamat et al. (2016), and accounting for varying surface heat fluxes Gu et al. (2022); Muñoz-Criollo et al. (2016).

Similar to the modelling of the ground, models of varying complexity are used for the pipes and fluid flow. In the simplest case, a linear temperature profile between inlet and outlet is assumed for a steady state condition (e.g., Kavanaugh and Rafferty (2014)). A more complex analytical solution considers the nonlinear temperature profile along the pipe Van Genuchten (1982). Assuming a homogeneous temperature field in the fluid cross section, transient fluid flow can be modelled with one-dimensional numerical models. The coupling of the fluid models and the surrounding ground is then done through a series of thermal resistances accounting for the convective resistance from the fluid to the pipe and the conductive resistance of the pipe.

Since multiple models exist, it is hard to assess what modelling approaches to use that is suitable for a range of realistic conditions. The published literature suggests that the horizontal connection pipes can have a significant influence on the BHE operation. The level of impact may be a function of climate, depth and thermal loads, for which reliable models are needed. Depending on the conditions, the horizontal connection pipes can have a beneficial effect due to heat gains and may lead to reduced required BHE length and, therefore, cost. If the heat losses predominate, neglecting the horizontal pipes in the design may result in reduced efficiency of the entire system. While 3D numerical modelling or physical experiments are well-suited in an academic context, simpler models are usually preferred for practical applications. Hence, the aim of this work is to identify simulation models suited to investigate heat transfer along horizontal connection pipes and to develop a computationally efficient and simple methodology that is appropriate to capture these effects. Three ground and three pipe models are studied. All model combinations are coupled with a GSHP model. Figure 1 schematically shows the typical arrangement for GSHP systems and the associated models and nomenclature used in
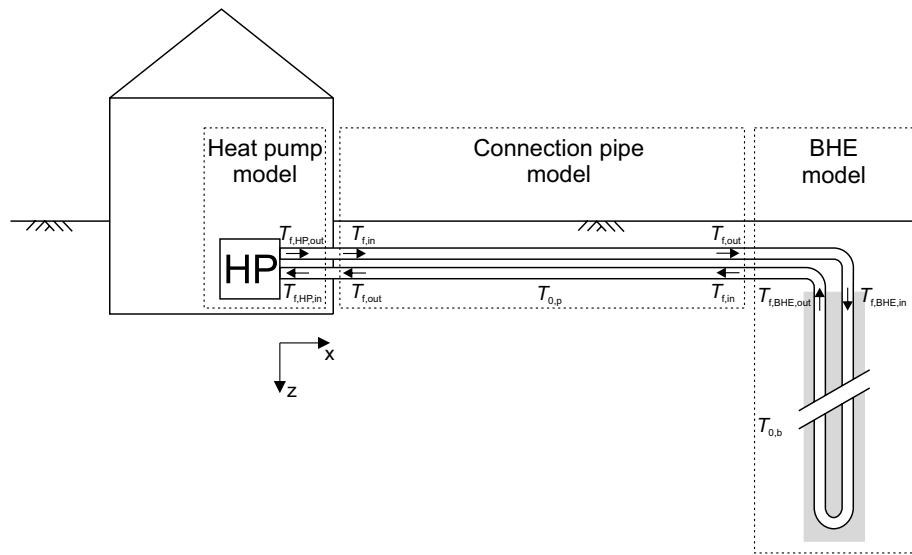
Düber *et al. Geothermal Energy*   (2023) 11:15

Page 4 of 32

Fig. 1 Schematic illustration of the simulated system and the coupled models

the article. The models used for the ground and pipes are described in "Models" section and are available through a GitHub repository. In "Scenarios" Section , the investigated scenarios are presented, followed by the results and discussion in "Results" and "Conclusions" Sections.

Models

Pipe models

The one-dimensional heat transfer along a buried pipe is described by Eq. 1. The heat capacity of the pipe wall is neglected, and heat is exchanged with the surrounding ground:

$$\frac{\partial T_f}{\partial t} + u_f \frac{\partial T_f}{\partial x} - \alpha_f \frac{\partial^2 T_f}{\partial x^2} + \phi(T_f - T_s) = 0. \tag{1}$$

T_f and T_s are the temperatures of the fluid and the soil, u_f is the velocity of the fluid and α_f its thermal diffusivity. The specific heat transfer coefficient ϕ is calculated based on the thermal resistance between fluid and soil R_{fs}, the volumetric heat capacity of the fluid ρc_f and the inner cross-sectional area of the pipe A_i:

$$\phi = \frac{1}{R_{fs} A_i \rho c_f}. \tag{2}$$

R_{fs} is the sum of the convective resistance between fluid and inner pipe wall, R_{conv}, and the conductive resistance of the pipe wall, R_p (see Fig. 2). The latter is calculated as

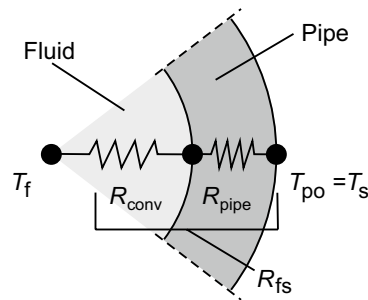$$R_p = \frac{\ln(r_{p,i}/r_{p,o})}{2\pi \lambda_p} \tag{3}$$

Düber *et al. Geothermal Energy*   (2023) 11:15

Page 5 of 32

Fig. 2 Thermal resistances between fluid and soil

where $r_{p,i}$ is the inner radius of the pipe and $r_{p,o}$ its outer radius while λ_p denotes its thermal conductivity Carslaw and Jaeger (1959).

The convective resistance R_{conv} is calculated with the dimensionless flow coefficients *Reynolds, Nusselt* and *Prandtl* Gnielinski (2013):

$$R_{conv} = \frac{1}{Nu\lambda_f\pi} \tag{4}$$

$$Re = \frac{u_f d_{p,i}}{\eta_f/\rho_f} \tag{5}$$

$$Pr = \frac{\eta_f c_f}{\lambda_f} \tag{6}$$

The formula for Nusselt number depends on the flow state. For laminar flow, the Nusselt number is defined as Gnielinski (2013):

$$Nu = 4.364. \tag{7}$$

For turbulent flows, the following applies:

$$Nu = \frac{(\zeta/8)RePr}{1 + 12.7\sqrt{\zeta/8}(Pr^{2/3} - 1)}\left[1 + \left(\frac{d_{p,i}}{l_p}\right)^{2/3}\right] \tag{8}$$

with:

$$\zeta = (1.8\log_{10}Re - 1.5)^{-2}, \tag{9}$$

while for flow in the transient region Eqs. 10 and 11 apply.

$$Nu = (1 - \gamma)4.364 + \gamma\left\{\frac{(0.0308/8)10^4 Pr}{1 + 12.7\sqrt{0.308/8}(Pr^{2/3} - 1)}\left[1 + \left(\frac{d_{p,i}}{l_p}\right)^{2/3}\right]\right\} \tag{10}$$

with:

$$\gamma = \frac{Re - 2300}{10^4 - 2300} \quad (0 \le \gamma \le 1). \tag{11}$$

Table 1 Properties of the investigated pipe models

Model	Axial temperatures	Transient flow
1D-numerical	✓	✓
Steady state	✓	✗
Steady state linear	✗	✗

Here $d_{p,i}$ is the inner diameter of the pipe, l_p the pipe length, η_f the dynamic viscosity of the fluid, ρ_f its density and c_f its specific heat capacity.

The lateral heat transfer between fluid and soil is calculated with the described resistance R_{fs} in all investigated pipe models, while three approaches with differing degrees of simplification are used for the heat transfer along the pipe axis (Table 1).

1D numerical model

The transient fluid flow with time-dependent fluid inlet and soil temperatures as boundary conditions can be captured with a numerical model. Here, we choose the Finite-Volume-Method (FVM) for the discretization of Eq. 1. Utilizing the upwind scheme, the fluid temperature at time step $i+1$ and cell x is calculated as:

$$T_f(x, t_{i+1}) = T_f(x, t_i) + \Delta t \frac{u_f}{\Delta x}[T_f(x-1, t_i) - T_f(x, t_i)] + \Delta t \phi [T_s(x, t_i) - T_f(x, t_i)].$$

(12)

Due to the explicit Euler scheme, the cell size Δx and the time step Δt must be chosen in a way that the CFL criterion is met: $\frac{u_f \Delta t}{\Delta x} \leq 1$.

Steady-state analytical model

For constant inlet fluid and soil temperatures, the analytical solution for Eq. 1 is given by Van Genuchten (1982):

$$
T_f(x, t) = T_s + \frac{(T_{f,in} - T_s)}{2} \left\{ \exp\left[\frac{(u_f - v)x}{2\alpha_f}\right] \text{erfc}\left(\frac{x - vt}{2\sqrt{\alpha_f t}}\right) \right.
$$
$$
\left. + \exp\left[\frac{(u_f + v)x}{2\alpha_f}\right] \text{erfc}\left(\frac{x + vt}{2\sqrt{\alpha_f t}}\right) \right\}
$$

(13)

with

$$v = u_f \sqrt{1 + \frac{4\phi\alpha_f}{u_f^2}}$$

(14)

where $\alpha_f = \frac{\lambda_f}{\rho c_f}$ is the thermal diffusivity of the fluid. In our study, the pipe models are coupled with various ground models as well as a BHE model and a highly simplified, yet sufficient, GSHP model imposing a ground load boundary condition. As a result, the inlet $T_{f,in}$ and ground temperatures T_s change in each calculation step, so that Eq. 13 cannot be used as it is only valid for constant inlet fluid temperatures. To simplify matters,

we assume that the pipe is completely flowed through in each calculation step and that a steady-state is reached. The steady-state solution for Eq. 13 reads as

$$T_{\mathrm{f}}(x) = T_{\mathrm{s}} + (T_{\mathrm{f,in}} - T_{\mathrm{s}}) \exp \left[\frac{(u_{\mathrm{f}} - v)x}{2\alpha_{\mathrm{f}}} \right] \tag{15}$$

and this simpler solution is implemented in the model in this work.

Steady-state linear model

Assuming stationary conditions and a linear temperature profile along the pipe, Eq. 15 can be further simplified to find the outlet temperature $T_{\mathrm{f,out}}$ of the horizontal connection pipe of length l_{p}:

$$T_{\mathrm{f,out}} = T_{\mathrm{f,in}} - (T_{\mathrm{f,in}} - T_{\mathrm{s}}) \frac{2\phi l_{\mathrm{p}}}{\phi l_{\mathrm{p}} + 2u_{\mathrm{f}}}. \tag{16}$$

To verify the correct implementation of the described pipe models, a comparative simulation was carried out with the finite-element software COMSOL Multiphysics®. A single 50m long pipe with an outer diameter of 40 mm, a wall thickness of 3.7 mm and a thermal conductivity of 0.37W m$^-$ K$^-$ was used. The fluid had a flow rate of 35m^{3}d^{-1} and a temperature entering the pipe of 30°C, while the temperature at the outer wall of the pipe is set to 15°C. The fluid has also a thermal conductivity of 0.598W m$^-$ K$^-$, a density of 998.23kgm^{-3}, specific heat capacity of 4184J kg^{-1}K^{-1} and a dynamic viscosity of 1.10016mP as. The results are shown in Fig. 3 for $t = 53.8$s, where the fluid has travelled 27m into the pipe (left) and $t = 103.8$s (right), which is a sufficiently long time for steady state conditions. The numerical models (COMSOL, 1D num.) suffer from numerical diffusion, leading to a smeared temperature front compared to the analytical solution (Fig. 3). For this example, the energy absorbed by the fluid during the first $t = 103.8$s is 399kJ for the transient models and 744kJ for the steady state linear model. Once pipe is flown through, the difference in heat exchange rate between the steady state linear model and all other models is only 75W.
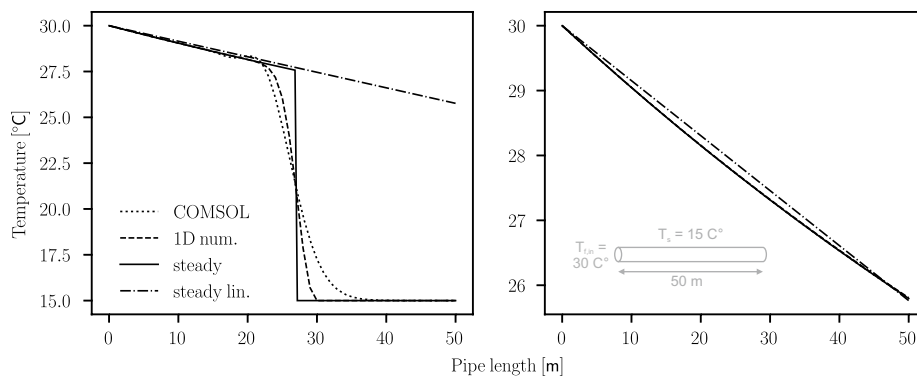

Fig. 3 Verification of the pipe model implementation: transient case with the temperature front at the middle of a 50m long pipe (left) and steady state case with fully flown through pipe (right)

Table 2 Investigated ground models: soil resistance model (R_s), finite line source model (FLS) and the two-dimensional numerical model with selected distinguishing features

Model	Temperature accumulation	Inhomogenous ground	Axial temperature field
2D numerical	✓	✓	X
FLS	✓	X	(✓)
R_s	X	X	X

Ground models

As the aim of this work is to investigate and develop simple models that are suitable for determining the heat losses along the connection pipes of BHEs, we limit the heat transfer processes in the ground to conduction, leading to Eq. 17 for the three-dimensional subsurface domain.

$$\frac{\partial}{\partial x}\left(\lambda \frac{\partial T}{\partial x}\right) + \frac{\partial}{\partial y}\left(\lambda \frac{\partial T}{\partial y}\right) + \frac{\partial}{\partial z}\left(\lambda \frac{\partial T}{\partial z}\right) + q_v = \rho c \frac{\partial T}{\partial t} \tag{17}$$

Here λ is the ground thermal conductivity (assumed to be the same in all directions), ρc the volumetric heat capacity and q_v the source term. As with the pipe models, we use three different models of varying complexity, as listed in Table 2.

2D numerical model

If heat transfer along the pipe axis is neglected, the first summand in Eq. 17 can be dropped and the ground described by a two-dimensional temperature field. We discretise the reduced version of Eq. 17 with the finite volume method. The central difference scheme is used to interpolate the temperatures on the cell walls. For adjacent cells with different thermal conductivities, the harmonic mean is applied to determine the mean thermal conductivity at the cell walls, i.e. a solution for heat transfer in media in series. We use the explicit Euler scheme for the numerical integration due to its simplicity and computational efficiency, leading to
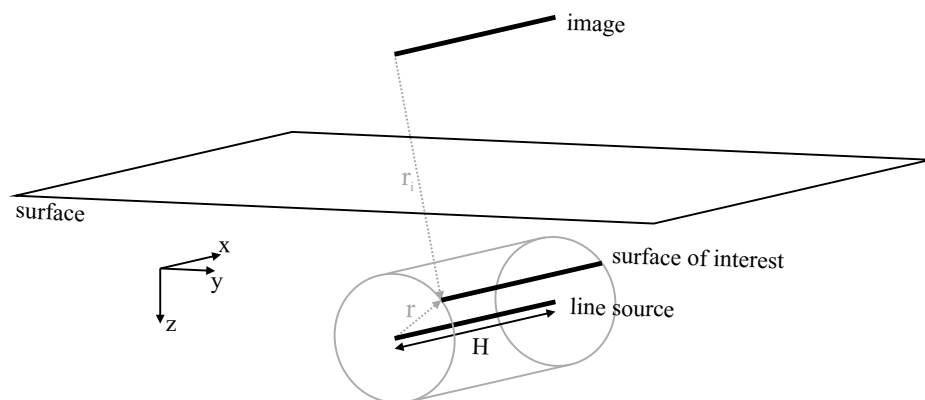

Fig. 4 Horizontal finite line source and the method of images

Düber *et al. Geothermal Energy*   (2023) 11:15

Page 9 of 32

$$
\begin{aligned}
T(y,z,t_{i+1}) =\ & T(y,z,t_i) + \frac{\Delta t}{\rho c(y,z)\Delta yz^2}\Big\{ \lambda_y(y{-}1,z)T(y{-}1,z,t_i) \\
& - \Big[\lambda_y(y{-}1,z) + \lambda_y(y,z) + \Big]T(y,z,t_i) + \lambda_y(y,z)T(y{+}1,z,t_i) \\
& + \lambda_z(y,z{-}1)T(y,z{-}1,t_i) \\
& - \Big[\lambda_z(y,z{-}1) + \lambda_z(y,z) + \Big]T(y,z,t_i) + \lambda_z(y,z)T(y,z{+}1,t_i) \\
& + q_v(y,z,t_i) \Big\}
\end{aligned}
\tag{18}
$$

with

$$
\lambda_y(y,z) = \frac{2}{\frac{1}{\lambda(y,z)} + \frac{1}{\lambda(y+1,z)}}
\tag{19}
$$

and

$$
\lambda_z(y,z) = \frac{2}{\frac{1}{\lambda(y,z)} + \frac{1}{\lambda(y,z+1)}}
\tag{20}
$$

where $\Delta y = \Delta z = \Delta yz$ is the regular cell size, λ the thermal conductivity and ρc the volumetric heat capacity.

Finite line source model

Lamarche Lamarche (2019) has presented the general solution for the horizontal finite line source in a half space to calculate segment-to-segment temperature responses. Similar to the work in Claesson and Javed (2011); Lamarche (2011), the method of images is used to account for the ground surface boundary condition (Fig. 4). The temperature change in the ground ΔT_s at the outer wall of a single segment pipe (the horizontal line source) can be calculated as

$$
\Delta T_s(t) = \frac{q}{4\pi\lambda}g(t)
\tag{21}
$$

with

$$
g(t) = \int_{\frac{1}{\sqrt{4\alpha t}}}^{\infty} \frac{2\left(e^{-r^2 s^2} - e^{-r_i^2 s^2}\right)}{s^2}\left[Hs\,\mathrm{erf}(Hs) - \frac{1}{\sqrt{\pi}}\left(1 - e^{-H^2 s^2}\right) \right]ds
\tag{22}
$$

where q is the length related heat load, λ the thermal conductivity of the soil and H is the length of the line source. r denotes the distance between the line source and the surface of interest (i.e., outer pipe wall) and r_i the distance between the imagery line source and the surface of interest (Fig. 4).

Superimposing the temperature change with the undisturbed ground temperature T_0 finally provides the ground temperature at the outer pipe wall T_s:

$$
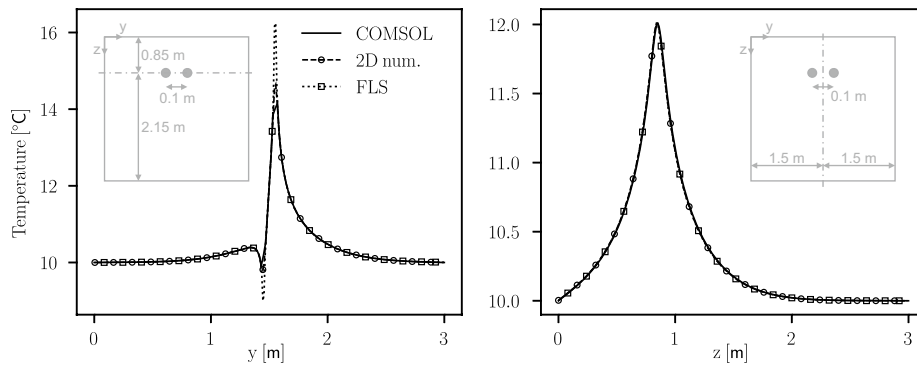T_s(t) = T_0(t) + \Delta T_s(t).
\tag{23}
$$

Fig. 5 Verification of the ground model implementation: horizontal (left) and vertical (right) temperature profile

By applying the superposition principle Carslaw and Jaeger (1959), time-variable thermal loads $q(t)$ can be considered as the source term (last summand in Eq. 17). Thus, the load profile with stepwise constant loads is transferred into load increments:

$$\Delta q(t_i) = q(t_i) - q(t_{i-1}) \tag{24}$$

and a summation over time applied, leading to

$$T_s(t_k) = T_0(t_k) + \frac{1}{4\pi\lambda} \sum_{i=1}^{k} \Delta q(t_i) \cdot g_p(t_{k-i+1}). \tag{25}$$

Soil resistance model

The work of Kavanaugh and Rafferty Kavanaugh and Rafferty (2014) provides a calculation template to estimate heat gain and loss in horizontal buried pipe headers. This model is identical to the FLS, but uses a different formulation for the line source. Furthermore, it does not consider temporal or spatial superposition. To include a similar model in the comparison here, we will implement Eq. 21-23, neglecting interference of multiple pipes and temperature accumulation in the ground.

To verify the implementation of the 2D numerical model and the FLS model, a comparative simulation was carried out against a full 3D finite-element model implemented in the package COMSOL Multiphysics®. For this purpose, a cylindrical heat source of $10\,\mathrm{W\,m^{-1}}$ and a cylindrical heat sink of $-5\,\mathrm{W\,m^{-1}}$ with diameters of 40mm were placed at $-0.85\mathrm{m}$ from the upper boundary in a 3×3 m 2D model with thermally insulated boundaries. Fig. 5 shows a horizontal (y) and vertical (z) temperature profile after a simulation time of 48h. The models show good agreement. Only the horizontal section shows deviations for the area within the heat sources. However, these areas are not relevant for the coupled simulations, as the interface to the pipe model is the ground temperature at the outer radius of the pipe.

Coupling of pipe and ground models

The coupling parameters between the pipe models and the ground models are the soil temperature at the pipe wall T_s and the heat flow between soil and pipe. Based on the soil temperature and the fluid inlet temperature $T_{f,in}$, the pipe models calculate new fluid outlet temperatures $T_{f,out}$ and the fluid temperatures along the horizontal pipe. The difference between the mean fluid temperature within the pipe $\overline{T}_f$ and the temperature at the soil-pipe wall interface T_s and the thermal resistance between fluid and soil R_{fs} determine the ground load:

$$q = \frac{T_s - \overline{T}_f}{R_{fs}}. \tag{26}$$

The ground load serves as input for the ground models to calculate the soil temperature at the pipe wall. As the soil temperature at the pipe wall depends on the fluid temperature which also depends on the pipe wall temperature, this problem requires an iterative scheme as shown in Fig. 6. As a first guess for the soil temperature, we use the value from the previous timestep $i-1$. After calculating a new ground temperature, this process is repeated, until an error tolerance criterion is fulfilled. The deviation of the outlet fluid temperature between two iterations is used as error criterion:

$$e = \left| \frac{T_{f,out}^{new} - T_{f,out}^{old}}{T_{f,out}^{old}} \right|. \tag{27}$$

The combination of coupled pipe and ground model will henceforth be referred to as the connection pipe model. For the investigations carried out, the various connection pipe models are coupled with a BHE model on the one side and a fixed thermal load boundary condition representing the heat pump on the other side as shown in Fig. 1.

BHE model and thermal load boundary condition

For the BHE model, we use the work of Düber et al. Düber et al. (2022), since it is computationally efficient and can be easily coupled with the connection pipe models through its implementation in Python. The model follows the idea of Wetter and Huber Wetter and Huber (1997) of combining a semi-numerical borehole model with a g-function ground model. The interaction of the BHEs and the consideration of time-variable loads
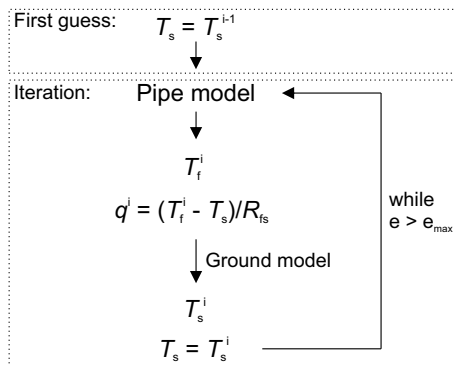
Fig. 6 Coupling scheme between ground and pipe models

are taken into account by spatial and temporal superposition. The borehole models utilize the thermal resistance capacity models from Bauer et al. Bauer et al. (2011) for the horizontal heat transfer and the finite volume method for the heat transfer in vertical direction. To overcome high computational times for simulations with many time steps, the model also uses the Fast Fourier Transformation and the convolution theorem for better efficiency Marcotte and Pasquier (2008).

One input parameter for the simulations will be the ground load presented in the next section. To impose the load as a boundary condition on the model, we use Eq. 28, acting as a highly simplified heat pump model. The outlet temperature of the heat pump $T_{f,HP,out}$ at time step i as is calculated as follows:

$$T_{f,HP,out}(t_i) = T_{f,HP,in}(t_{i-1}) - \frac{q(t_i)}{\dot{V}\rho c_f} \tag{28}$$

where $\dot{V}$ is the volumetric flow rate of the fluid and ρc_f its volumetric heat capacity. $T_{f,HP,in}(t_{i-1})$ is the fluid inlet temperature of the heat pump (Fig. 1) and equal to the mean outlet temperature of all return horizontal connection pipes (i.e., the mean of all $T_{f,out}$). $q(t_i)$ is the ground load of the current time step.

For the simulations with six BHEs considered operating in parallel (see section 3), we make some assumptions that allow us to isolate and analyse the effect of the thermal interference of multiple horizontal connection pipes in a shared trench. While we recognize that turns and merging of connection pipes may also exist in real projects and thus differ from this arrangement, all pipes are assumed parallel along their entire length and arranged as shown in Fig. 7. Considering parallel operation, all supply connection pipes are assumed to be connected to the same heat pump, thus receiving the same inlet temperature $T_{f,HP,out}$, while $T_{f,HP,in}$ is the the mean of all $T_{f,out}$ (Fig. 1). On the other side, each pair of connection pipes is connected to an individual BHE, however the BHE models are set up to have no thermal interference between them.
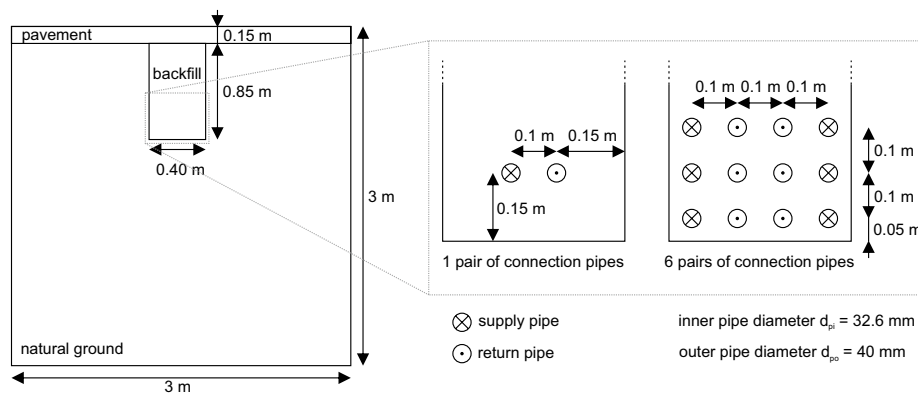

Fig. 7 Cross-section of the trench for the heterogeneous ground model and pipe arrangement

Table 3 Thermal properties of the trench and connection pipe

	λ [W m^{-1} K^{-1}]	ρc [J m^{-1} K^{-1}]
Natural ground	1.5	18,00000
Backfill	0.9	15,00000
Pavement	1.2	16,00000
Pipe	0.38	–

Scenarios

The model comparison is carried out using scenarios with horizontal connecting pipes of 30 and 60m length and a single pair of pipes (1 BHE) or six pairs of pipes (6 BHEs) installed in a shared trench as shown in Fig. 7.

The properties of the horizontal pipes and the trench are listed in Table 3. The BHE data listed in Table 4 and the load profile shown in Fig. 8 (top) are from a study from Ahmadfard and Bernier Ahmadfard and Bernier (2019). The load profile corresponds to a building located in Atlanta and is scaled down for a single BHE with factor of 1/25 and 6/25 for the simulation with 1 and 6 BHEs, respectively.

Daily values for the air temperature in Atlanta serve as temperature boundary condition at the ground surface (Fig. 8, bottom). Temperatures at 3 m depth and the depths of the pipes have been calculated using a one-dimensional ground model with the thermal properties of the natural ground and the air temperature as surface temperature. The yearly cycle was repeated until a cyclic steady state was reached. For the numerical ground model, the temperatures at $z = \pm 0$m and $z = -3$m are used as boundary

Table 4 BHE and ground properties

| Parameter	Value	Units
Fuild properties		
Thermal conductivity	0.468	W m^{-1} K^{-1}
Density	1026	kg m^{-3}
Volumentric heat capacity	4123,494	J m^{-3} K^{-1}
Dynamic viscosity	0.00337	Pa s
BHE geometry		
Length	120	m
Diameter	0.150	m
Shank space	0.083	m
Outer diameter pipes	0.0334	m
Pipe wall thickness	0.0037	m
BHE-properties		
Thermal conductivity grout	2.0	W m^{-1} K^{-1}
Volumetric heat capacity grout	3900000	J m^{-3} K^{-1}
Thermal conductivity pipe	0.4	W m^{-1} K^{-1}
Ground properties		
Average thermal conductivity	1.9	W m^{-1} K^{-1}
Average volumetric heat capacity	2052000	J m^{-3} K^{-1}
Undisturbed ground temperature	15.0	°C
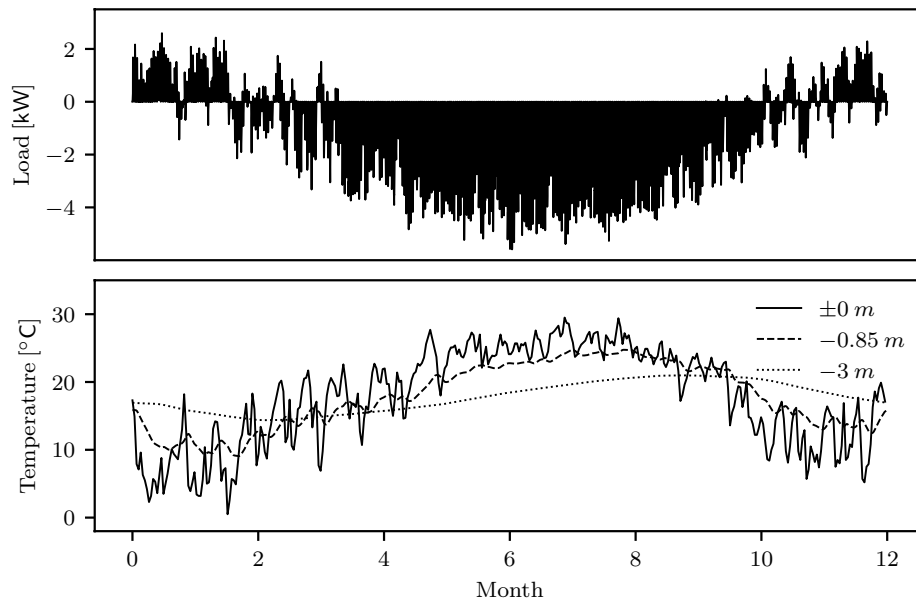
Fig. 8 Thermal load (top) and temperatures (bottom) used as boundary conditions

conditions at the top and the bottom of the model while the sides are considered thermally insulated.

In the FLS model, the temperature change due to heat exchange with the pipes is superimposed on the undisturbed temperature calculated at the depth of the pipes (e.g., −0.85 m), whereas in the soil resistance model, this temperature is used as a first order boundary condition.
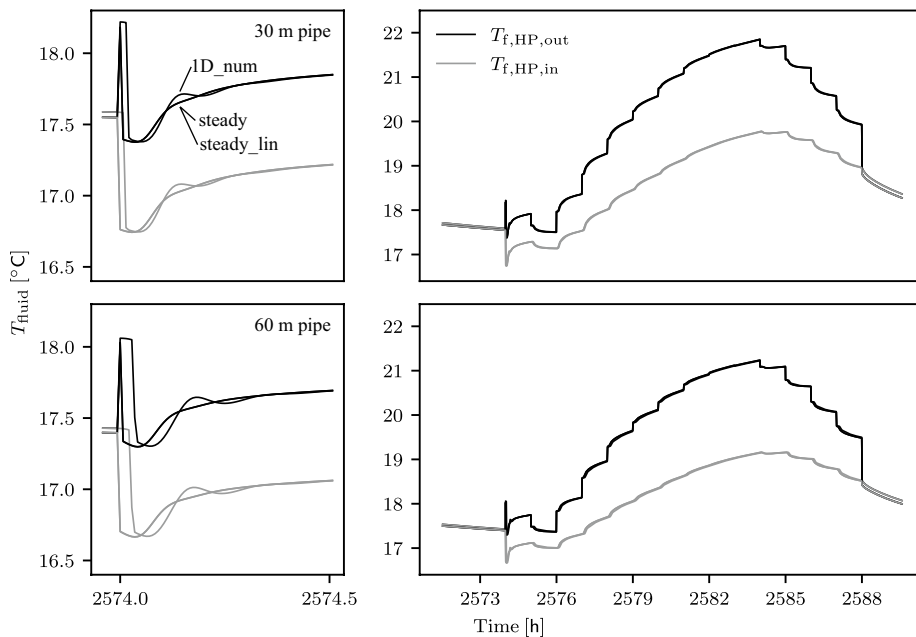

Fig. 9 Comparison of the pipe models in combination with the 2D numerical ground model with homogenous properties for 30m (top) and 60m (bottom) pipe lengths
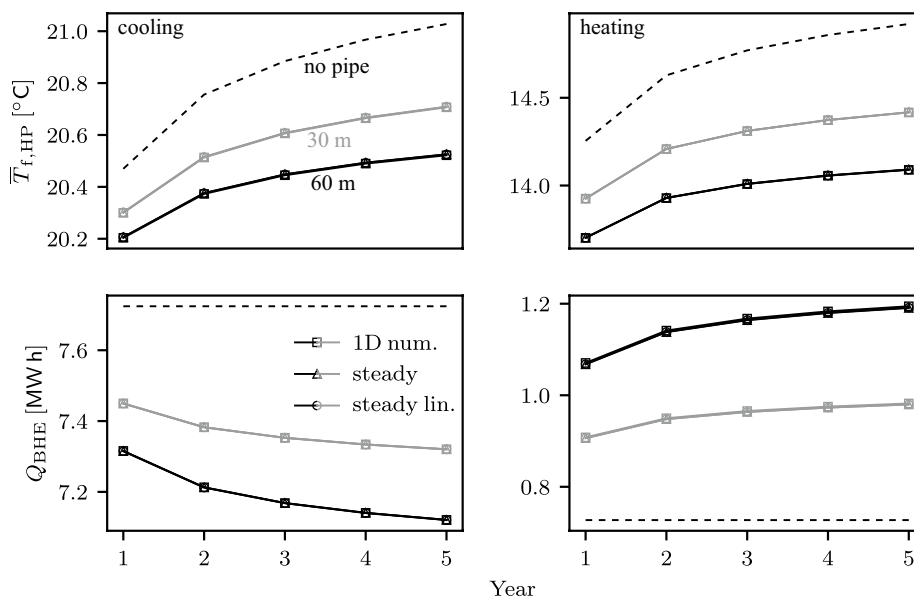
Düber *et al. Geothermal Energy*   (2023) 11:15

Page 15 of 32

Fig. 10 Effect of the pipe models on the annually averaged fluid temperatures (top) and on the amount of energy exchanged by BHE (bottom) separately for cooling (left) and heating (right)

The inhomogeneous properties of the ground as shown in Fig. 7 can be only considered in the 2D numerical ground model. All other models assume homogeneous conditions. For this reason, we apply the material properties listed in Table 2 to the numerical model to simulate the inhomogeneous case and the properties of the natural ground for the whole model to simulate the homogeneous case.

The numerical ground models were discretised with a cell size of $1 \times 1\,\mathrm{cm}$ and a time step of 25s. The numerical pipe model is discretised with 11 cells for the 30 m pipe length and 22 cells for the 60 m pipe length using a 5 s time step, resulting in a CFL-number of 0.89. In the analytical steady state model, the fluid temperatures are calculated at the same points as in the numerical model, while in the linear steady state model, the fluid temperature is calculated just at the outlet of the connection pipe (Fig. 1).

Results

Fluid temperatures and BHE loads

We use the scenario with one pair of connection pipes and the 2D numerical ground model with homogeneous properties for the comparison of the pipe models. Figure 9 shows the calculated fluid temperatures at the heat pump for a randomly selected section of approximately 15 h during cooling operation. For both the 30 m connection pipe (Fig. 9, top) and the 60 m connection pipe (Fig. 9, bottom), the calculated fluid temperatures are similar for all pipe models. The left part of Fig. 9, however, shows the first 30 min after the ground source heat pump starts to operate. Here, differences between the transient numerical pipe model and the two steady state models become apparent. In the numerical model, the actual travel time of the fluid through the connection pipes is considered correctly. Therefore, it takes longer for the outlet temperature to change, as the fluid in the pipe, which has the same temperature as the surrounding soil, is first

pushed to the outlet. This delay is exactly twice as long for 60 m pipe length as for the 30 m pipe length (Fig. 9, left).

To quantify the influence of the pipe models on the long-term operation of the BHE and the heat pump, average fluid temperatures $\overline{T}_{f,HP}$ at the heat pump and the energy exchanged between BHE and ground Q_{BHE} are investigated for a period of 5 years (Fig. 10). The evaluation is carried out separately for heating and cooling operation. $\overline{T}_{f,HP}$ is the annual average of the mean of the fluid temperatures entering and exiting the heat pump.

The long-term observation also reveals no relevant differences between the models in terms of temperature. For the scenarios with 60 m pipes, the average fluid temperatures for both heating and cooling are 0.2–0.3K lower than for the 30 m pipes which are around 0.4K lower than for the reference case with no horizontal connection pipes. These seeimingly small variations in temperature may have significant thermal energy variations implications, particularly during the 25+ years life-span of HVAC systems.

During the cooling operation, the energy injected into the ground per year through the BHE decreases from 7.7 MW h (reference case without pipes) to 7.3 MW h for the case with 30 m connection pipes and to 7.1 MW h for the case with 60 m pipes in the fifth year of operation. For heating operation, the energy extracted through the BHE increases from 0.7 MW h to just under 1 MW h for 30 m connection pipe length and to 1.2 MW h for 60 m connection pipe length. The absolute energy losses along the connection pipes are comparable for heating and cooling operation. However, comparted to the reference case, the relative increase for the heating operation is significantly higher. The evaluation of the annual average values shows that the short-term differences between the transient numerical model and the stationary models have no influence on parameters relevant for plant design. For this application, all investigated pipe models are therefore equally well suited.

A first comparison of the ground models is carried out using the scenarios with the 1D numerical pipe model and 30 m connection pipe length. Figure 11 shows a section of the calculated fluid temperatures. With the exception of the soil resistance model (R_s),
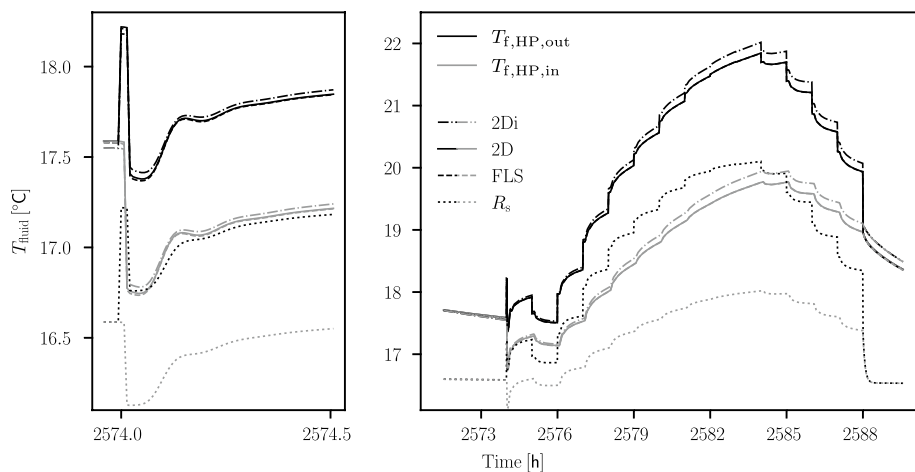

Fig. 11 Comparison of the ground models in combination with the 1D numerical pipe model for 30 m pipe length during a day after the first 100 days of operation of the GSHP system
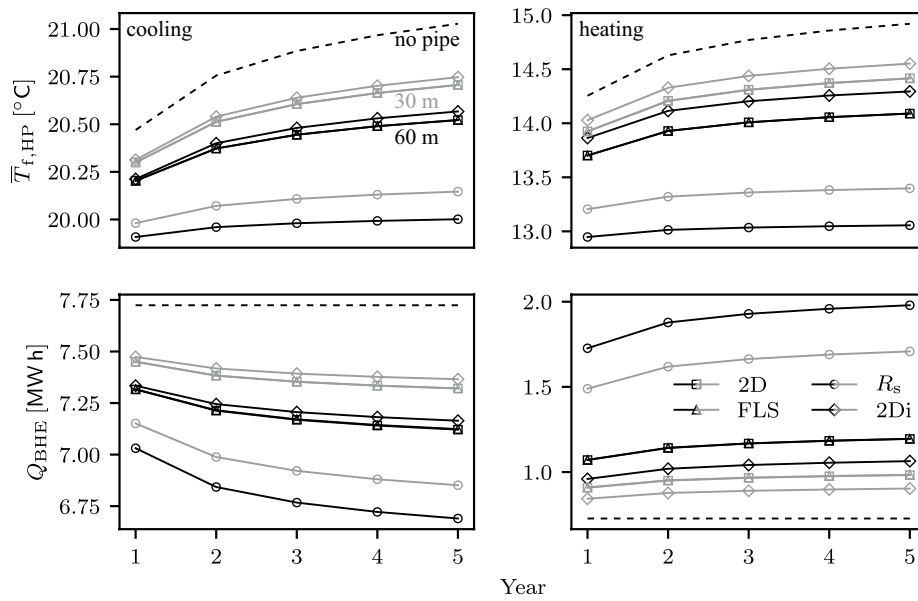
Fig. 12 Effect of the ground models on the annually averaged fluid temperatures (top) and on the amount of energy exchanged by BHE (bottom) separately for cooling (left) and heating (right) for a 30 m (grey) and 60 m horizontal connection pipe

the deviations between all models are relatively small. As expected, the FLS model and the numerical 2D model with homogeneous properties (2D) produce almost identical results. The difference to the numerical 2D model with inhomogeneous properties (2Di) increases with continued operation and larger loads, but remains below 0.2K within the shown period. The fluid temperatures calculated with the soil resistance model are almost 2K below all other models. During the first 2500 h of operation, both inlet and outlet temperatures are in any model higher than the undisturbed ground temperature around the connection pipes. This leads to a heat accumulation in the ground, resulting in higher fluid temperatures for the models accounting for heat accumulation.

Figure 12 shows the long-term evaluation of the ground models similar to Fig. 10. Regardless of the pipe length no visible differences between the 2D numerical model with homogeneous properties and the FLS model for both the fluid temperatures and the exchanged energy can be observed. During cooling operation, the difference in mean fluid temperature between the inhomogeneous and homogeneous 2D models in the fifth year is about 0.05K for both pipe lengths, while for the heating operation, it is 0.2K. The difference between 30 m and 60 m pipe is not more than 0.3K for any ground model. The most significant deviation from all other models as well as from the reference case is produced by the soil resistance model. For example, for the 30 m pipe model, the mean fluid temperature during the cooling operation is 1K lower as in the reference case without any pipes, while it is 1.5K lower for the heating operation.

The difference between the homogeneous and inhomogeneous model in cooling operation is less than 0.05 MW h per year for both pipe lengths tested. Q_{BHE} calculated with the R_s model is approx. 0.5 MW h below the other models for cooling and 0.7 MW h above them for heating.
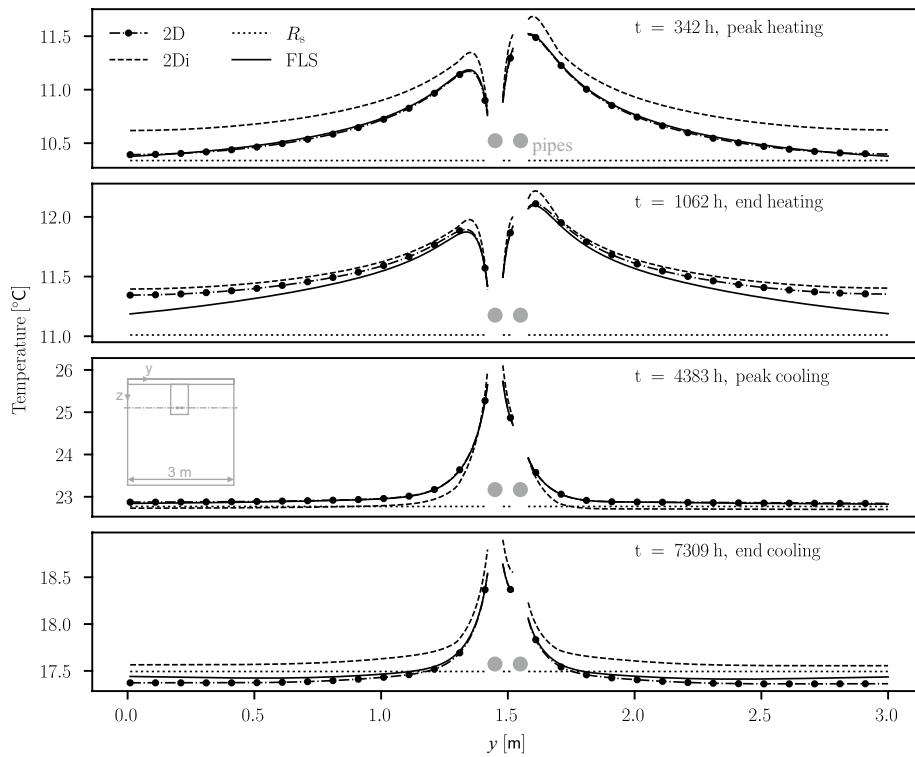
Fig. 13 Horizontal temperature profile at the depth of the connection pipes at selected times during the first year of operation, calculated with the 1D numerical pipe model for 30 m pipe length
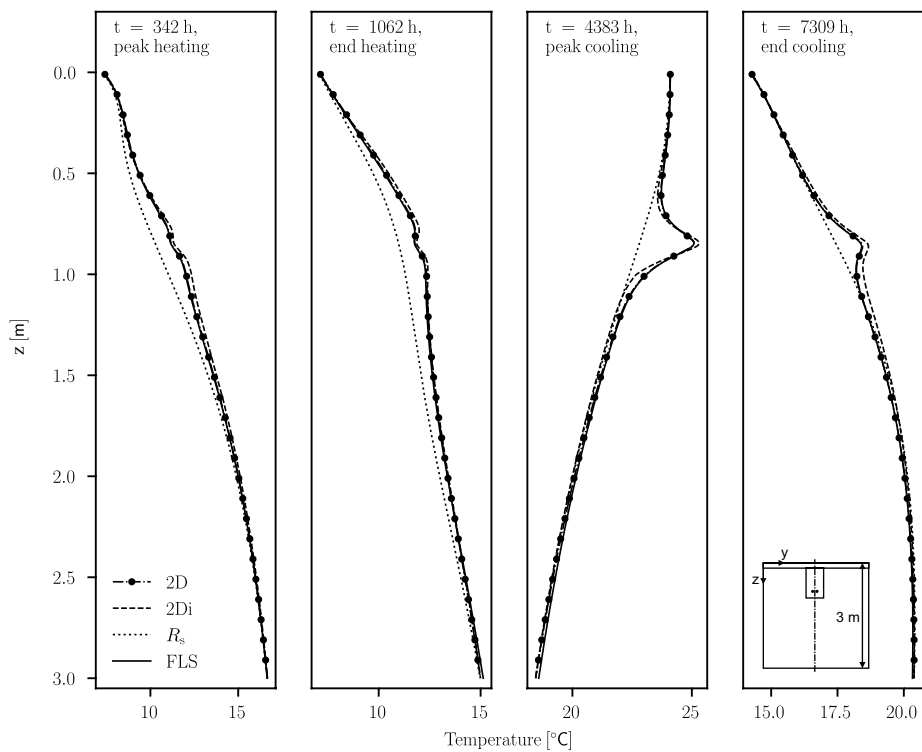

Fig. 14 Vertical temperature profile between the supply and return pipe at selected times during the first year of operation, calculated with the 1D numerical pipe model for 30 m pipe length

In addition to the fluid temperatures and the energy exchanged through the BHE, we can also compare the ground temperatures calculated with the different models. The comparison is made at the following events: the maximum heating and cooling load as well as the end of the heating and cooling period. Figure 13 shows the temperature profile along a horizontal section at the depth of the connection pipes, while Fig. 14 shows a vertical section between the supply and return pipe. Since in the soil resistance model (R_s), the ground temperature is not influenced by the pipes, it corresponds to the undisturbed ground temperature. The temperatures calculated with the FLS model and the homogeneous 2D model are largely congruent. One exception are the temperature profiles in the horizontal section at the end of the heating period (Fig. 13, second from top). Here, the temperatures diverge with increasing distance from the pipes. This indicates that the dimensions of the numerical model were chosen too small, as the temperature increase at the boundary of the model is higher than in the FLS model. For the analysis of the fluid temperatures and the BHE operation, however, this has no influence, as previously shown. The biggest change in the undisturbed ground temperature occurs within the selected times at the time of the maximum cooling load with more than 3K (Fig. 13, third from top).

The investigations on a single BHE with connection pipes of 30 and 60 m length have shown that there are no significant differences with regard to the average fluid temperatures and BHE loads for the different ground models, with the exception of the soil resistance model. For homogeneous soil conditions, the FLS model and the 2D numerical model deliver identical results; for the numerical model, the geometry must be sufficiently large to ensure accurate results. For the scenario with the inhomogeneous soil conditions, the calculated temperatures deviate as expected, but the influence on the average fluid temperatures and BHE loads is negligible for the parameters investigated and a design-oriented view. The results of all model combinations for one pair of connection pipes are given in the Appendix.

For the scenarios with 6 BHEs, leading to 12 horizontal connection pipes in the same trench, nothing new is expected with regard to differences between the pipe models;
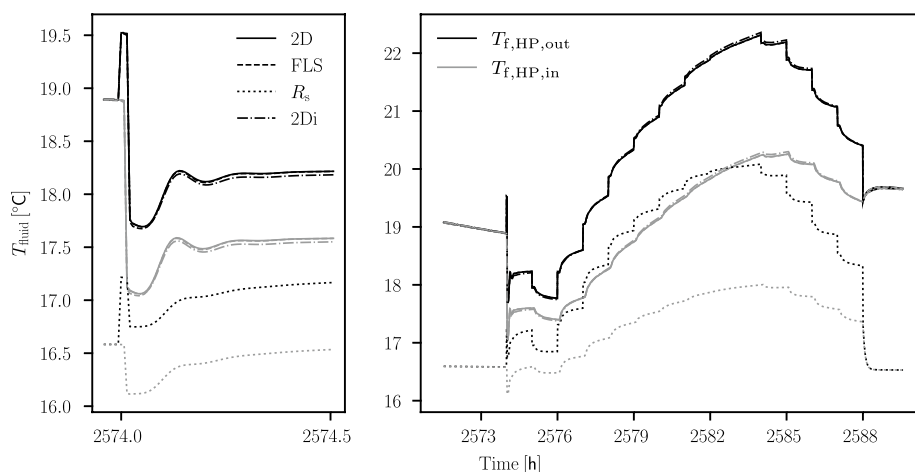

Fig. 15 Comparison of the ground models in combination with the 1D numerical pipe model for 30 m pipe length for the connection pipes of 6 BHEs in a shared trench
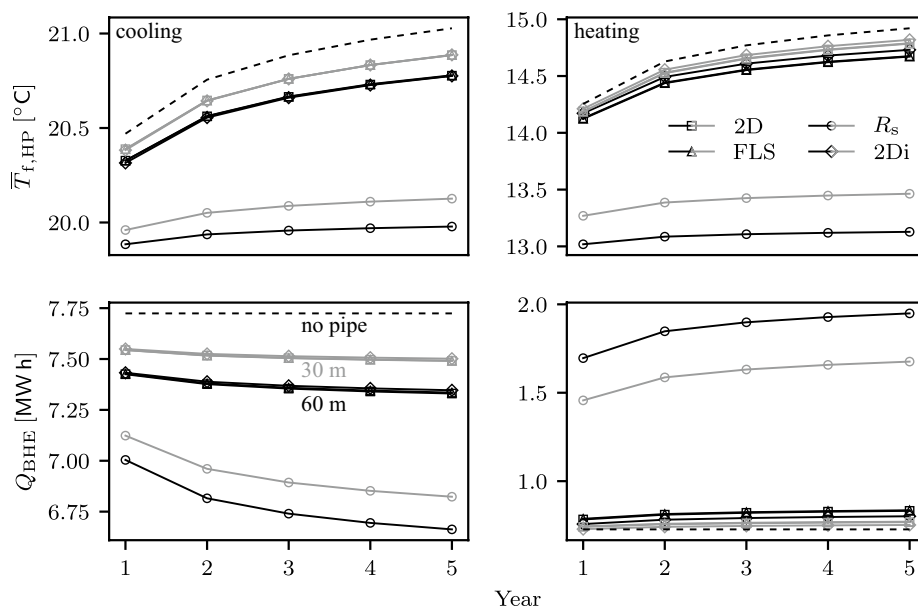
Fig. 16 Effect of the ground models on the annually averaged fluid temperatures (top) and on the amount of energy exchanged by BHE (bottom) separately for cooling (left) and heating (right) for the connection pipes of 6 BHEs in a shared trench
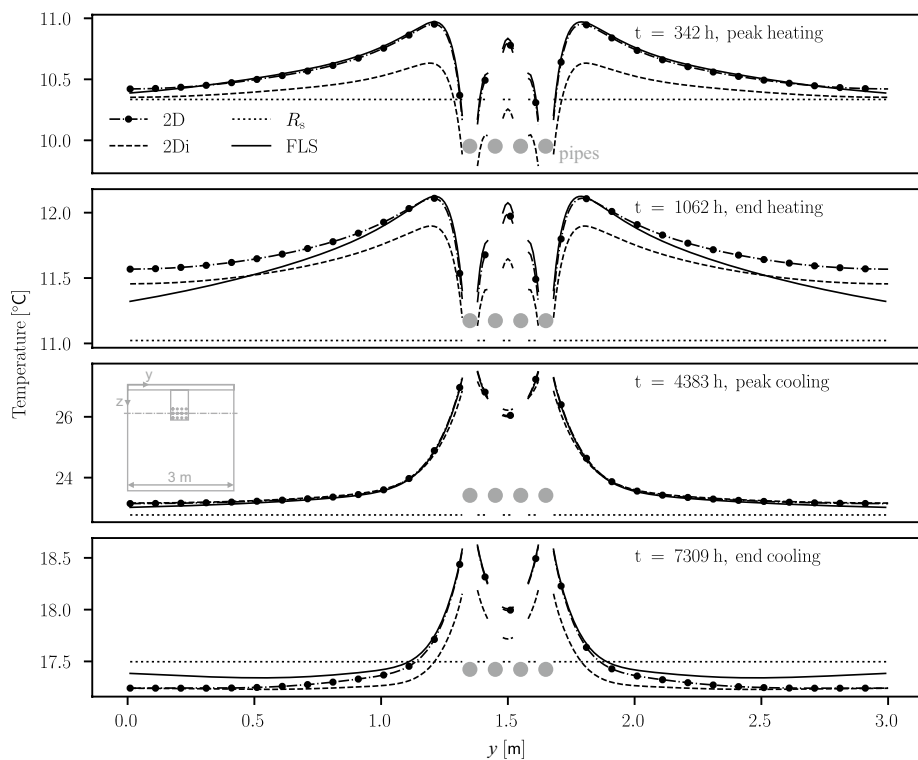

Fig. 17 Horizontal temperature profile at the depth of the connection pipes at selected times during the first year of operation, calculated with the 1D numerical pipe model for 30 m pipe length and 6 BHEs
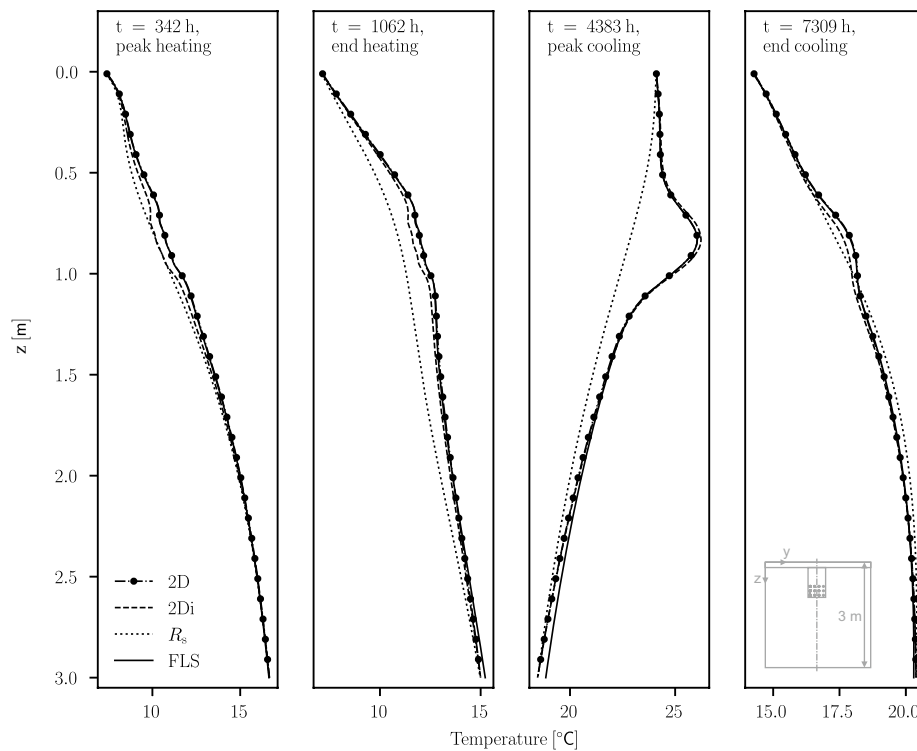
Fig. 18 Vertical temperature profile between the supply and return pipe at selected times during the first year of operation, calculated with the 1D numerical pipe model for 30 m pipe length and 6 BHEs

therefore, they are not discussed in more detail. Figure 15 shows the evaluation for the fluid temperatures at the heat pump analogous to Fig. 11. The heat pump inlet temperature is the average from all 6 BHE return connection pipes, the same applies for the BHE loads. Compared to the simulations with only one BHE, the difference between the homogeneous ground model and the inhomogeneous ground model is significantly lower with 6 BHEs. This is probably due to the fact that the distance of many pipes to the natural ground is smaller than in the simulation with only one BHE (Fig. 7). Furthermore, the fluid temperatures in all models except the soil resistance model are slightly higher (0.3K) as in the case with one pair of pipes. The comparison with the reference case (no connection pipes) in Fig. 16 reveals that multiple pipes reduce the effect of the connection pipes. Comparing Figs. 16 and 12 shows that for 6 pairs of pipes the values are much closer to the reference case for all models except the soil resistance model. By placing the pipes close together, each pipe has less thermally undisturbed soil volume around it, leading to a reduced heat exchange with the surrounding soil. This is also visible in the horizontal section through the middle row of pipes in Fig. 17: the inner return pipes are shielded by the outer supply pipes and are influenced by them more than by the undisturbed ground temperature. Figure 18 shows the temperature profiles for a vertical section between the pipes. The results of all model combinations for six pairs of connection pipes are presented in the Appendix.

The comparison of the ground models has shown that both FLS and the 2D numerical model are well suited for the application investigated in this work. Both models deliver identical results for homogeneous soil conditions for both pipe lengths investigated.

Table 5 Computational times for a 1 year simulation for the different pipe models in combination with the soil resistance model

Model combination	Comp. time
R_s + steady lin.	200s
R_s + steady	231s
R_s + 1Dnum	278s

Inhomogeneous soil conditions cannot be covered with the FLS model; the extent of their influence on the results depends on the actual conditions. In the example shown here, temperature accumulations occurred in the ground due to heat exchange with the connection pipes. The accumulations are not considered in the soil resistance model, leading to significant deviations that do not reflect reality. The arrangement of several connection pipes in a shared trench has shown that the heat exchange per pipe decreases significantly, leading to a reduced effect of the connection pipes on the heat pump and BHE operation altogether.

Computational effort

The comparison of the computational effort of the different models is carried out with the help of measured computational times where the processing unit is an Intel i7−7700K processor at 4200 MHz, 16 GB of RAM and Windows version 10. It is difficult to perform a fair and general comparison, as among the investigated models are both analytical, and thus discretization independent, and numerical models whose computational effort depends on the spatial discretization. Another influencing factor is the implementation. All models were implemented in Python to the best of our knowledge, but the authors are not professional programmers. The results shown are, therefore, only rough indications. Table 5 shows the computational times for the three pipe models in combination with the soil resistance model for a simulation time of 1 year at a time step of 25 s for a 60 m pipe. The computational times increase according to the complexity of the models.

The results for the different ground models are listed in Table 6. Again, the computational times increase with the complexity of the models. Due to the temporal and spatial superposition in the FLS model, the computational effort increases exponentially with the increasing number of time steps as well as increasing number of pipes. Comparing the times of the 1 BHE and 6 BHE simulations shows a factor of 7.5 for the soil resistance model, 24.5 for the FLS model and 3 for 2D numerical model. If more pipes are added

Table 6 Computational times for a 1 year simulation for the different ground models in combination with the steady-state linear pipe model

Model combination	Comp. time 1 BHE	Comp. time 6 BHEs
R_s + steady lin.	200s	1563s
FLS + steady lin.	396s	9722s
2D + steady lin.	6573s	19458s

or the number of time steps is increased, the 2D numerical model might perform better than the FLS model in terms of efficiency.

Proposed model

The study has shown that the steady state pipe model and the FLS ground model are sufficient for many cases. The BHE can be modeled with a similar approach Eskilson (1987):

$$T_{f,BHE,in}(t) = \overline{T}_f(t) + \frac{l_b q_b(t)}{2\dot{V}\rho c_f} \tag{29}$$

$$T_{f,BHE,out}(t) = \overline{T}_f(t) - \frac{l_b q_b(t)}{2\dot{V}\rho c_f} \tag{30}$$

$$\overline{T}_f(t) = q_b(t)R_b + T_b(t) \tag{31}$$

$$T_b(t_k) = T_{0,b} + \frac{1}{2\pi \lambda_s} \sum_{i=1}^{k} \Delta q_b(t_i) \cdot g_b(t_{k-i+1}). \tag{32}$$

Here, T_b denotes the borehole wall temperature, $T_{0,b}$ the undisturbed ground temperature of the borehole and q_b the stepwise constant borehole load divided by its length l_b. $\Delta q_b(t_i) = q_b(t_i) - q_b(t_{i-1})$ defines the load increment of each time step. g_b is the borehole g-function, $\overline{T}_f$ the average of the borehole inlet and outlet fluid temperatures, $\dot{V}$ is the volume flow and ρc_f the volumetric heat capacity of the fluid. The borehole resistance R_b is the effective thermal resistance of the BHE Javed and Spitler (2016).

Rewriting the equations for the steady-state pipe model combined with the FLS ground model leads for the case of one pair of connection pipes to:

$$q_{p1}(t) = \left[T_{f,BHE,in}(t) - T_{s1}(t)\right]\left(R_{fs} - \frac{l_p}{2\dot{V}\rho c_f}\right)^{-1} \tag{33}$$

$$q_{p2}(t) = \left[T_{f,BHE,out}(t) - T_{s2}(t)\right]\left(R_{fs} + \frac{l_p}{2\dot{V}\rho c_f}\right)^{-1} \tag{34}$$

and:

$$T_{s1}(t_k) = T_{0,s1}(t_k) + \sum_{i=1}^{k} \Delta q_{p1}(t_i) \cdot g_{p11}(t_{k-i+1}) + \Delta q_{p2}(t_i) \cdot g_{p21}(t_{k-i+1}) \tag{35}$$

$$T_{s2}(t_k) = T_{0,s2}(t_k) + \sum_{i=1}^{k} \Delta q_{p2}(t_i) \cdot g_{p22}(t_{k-i+1}) + \Delta q_{p1}(t_i) \cdot g_{p12}(t_{k-i+1}). \tag{36}$$

Here, index 1 corresponds to the supply pipe while 2 corresponds to the return pipe. q_p are the loads of the pipes divided by the pipe length l_p while $\Delta q_p(t_i) = q_p(t_i) - q_p(t_{i-1})$ defines the load increment for each time step. T_s is the soil temperature at the outside of

Düber *et al. Geothermal Energy*   (2023) 11:15

Page 24 of 32

the the pipes. The first index at the pipes g-function g_p corresponds to the heat source and the second to the surface of interest (Fig. 4).

The total load of the system of borehole and connection pipes Q_{tot} is defined as:

$$Q_{tot}(t) = q_{p2}(t)l_p + q_{p1}(t)l_p + q_{BHE}(t)l_b. \tag{37}$$

Combining Eqs. 29–37 into one matrix equation leads to:

$$\boldsymbol{A} \cdot \boldsymbol{B} = \boldsymbol{C} \tag{38}$$

with:

$$\boldsymbol{A} = \begin{bmatrix} 0 & 0 & -g_b(\Delta t) & 0 & 0 & 0 & 0 & 0 & 1 \\ 0 & 0 & R_b & 0 & 0 & 0 & 0 & -1 & 1 \\ 0 & 0 & +c_3 & 0 & 0 & -1 & 0 & 1 & 0 \\ 0 & 0 & -c_3 & 0 & 0 & 0 & -1 & 1 & 0 \\ -c_1 & 0 & 0 & -1 & 0 & c_1 & 0 & 0 & 0 \\ 0 & -c_2 & 0 & 0 & -1 & 0 & c_2 & 0 & 0 \\ 1 & 0 & 0 & -g_{p11}(\Delta t) & -g_{p21}(\Delta t) & 0 & 0 & 0 & 0 \\ 0 & 1 & 0 & -g_{p12}(\Delta t) & -g_{p22}(\Delta t) & 0 & 0 & 0 & 0 \\ 0 & 0 & l_b & l_p & l_p & 0 & 0 & 0 & 0 \end{bmatrix} \tag{39}$$

$$\boldsymbol{B} = \begin{bmatrix} T_{s1}(t_i) \\ T_{s2}(t_i) \\ q_b(t_i) \\ q_{p1}(t_i) \\ q_{p2}(t_i) \\ T_{f,BHE,in}(t_i) \\ T_{f,BHE,out}(t_i) \\ \overline{T}_f(t_i) \\ T_b(t_i) \end{bmatrix} \tag{40}$$

$$\boldsymbol{C} = \begin{bmatrix} \widetilde{T}_b(t_i) - q_b(t_{i-1})g_b(\Delta t) \\ 0 \\ 0 \\ 0 \\ 0 \\ 0 \\ \widetilde{T}_{s1}(t_i) - q_{p1}(t_{i-1})g_{11}(\Delta t) - q_{p2}(t_{i-1})g_{21}(\Delta t) \\ \widetilde{T}_{s2}(t_i) - q_{p2}(t_{i-1})g_{22}(\Delta t) - q_{p1}(t_{i-1})g_{12}(\Delta t) \\ Q_{tot}(t) \end{bmatrix} \tag{41}$$

and:

$$c_1 = \frac{1}{R_{fs} - \frac{l_p}{2\dot{V}\rho c_f}} \tag{42}$$

$$c_2 = \frac{1}{R_{fs} + \frac{l_p}{2\dot{V}\rho c_f}} \tag{43}$$

$$c_3 = \frac{l_b}{2\dot{V}\rho c_f}. \tag{44}$$

Equation 38 needs to be solved for $\boldsymbol{B}$ at each timestep t_i with a step size Δt. The temperatures in $\boldsymbol{C}$ are marked with a tilde as these are the initial undisturbed ground temperatures plus the temperature changes due to the previous time steps. These temperatures need to be updated according to the load increments of the current time step i for all future time steps $k > i$:

$$\widetilde{T}_b(t_k)^{new} = \widetilde{T}_b(t_k)^{old} + \Delta q_b(t_i) \cdot g_b(t_{k-i}) \tag{45}$$

$$\widetilde{T}_{s1}(t_k)^{new} = \widetilde{T}_{s1}(t_k)^{old} + \Delta q_{p1}(t_i) \cdot g_{p11}(t_{k-i}) + \Delta q_{p2}(t_i) \cdot g_{p21}(t_{k-i}) \tag{46}$$

$$\widetilde{T}_{s2}(t_k)^{new} = \widetilde{T}_{s2}(t_k)^{old} + \Delta q_{p2}(t_i) \cdot g_{p22}(t_{k-i}) + \Delta q_{p1}(t_i) \cdot g_{p12}(t_{k-i}). \tag{47}$$

For the simulation of additional BHEs and connecting pipes, the system of equations can be arbitrarily expanded. In contrast to many of the previous investigated model combinations, the proposed model requires no spatial discretization or internal iterations for the coupling, making it easy to implement and more efficient to run. The part for the horizontal pipes in the proposed model corresponds to the *FLS + steady state linear* combination. The computational time for the proposed model for the 1 year simulation is with just 205 s for one BHE almost halved (Table 6). Considering that the computational times listed in Table 6 do not include the computational time for the BHE model, which is in already included in the mentioned 205s, the savings with the new formulation are even higher. For the simulation with 6 BHEs, the new model needs just 10,023 s (again, including the BHEs) which is only little more than just the horizontal pipes model for this case (Table 6).

Figure 19 shows a comparison of the fluid temperatures calculated with the coupled hybrid approach used in the previous sections and the steady-state model (Eq. 38)
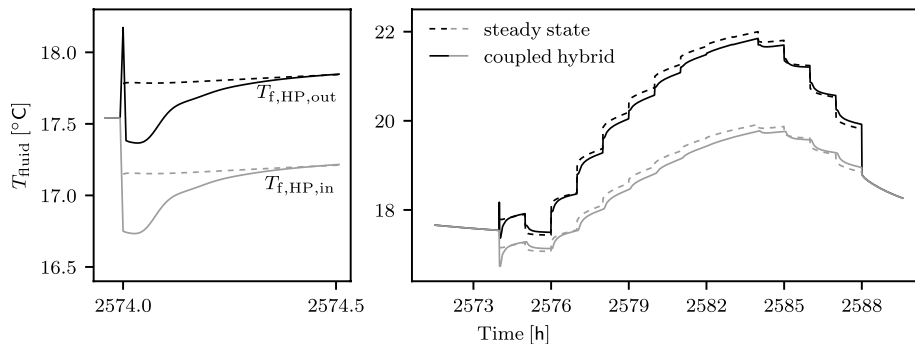

Fig. 19 Fluid temperature calculated with the proposed steady state approach and the coupled FLS ground and steady state pipe model for a 30 m connection pipe
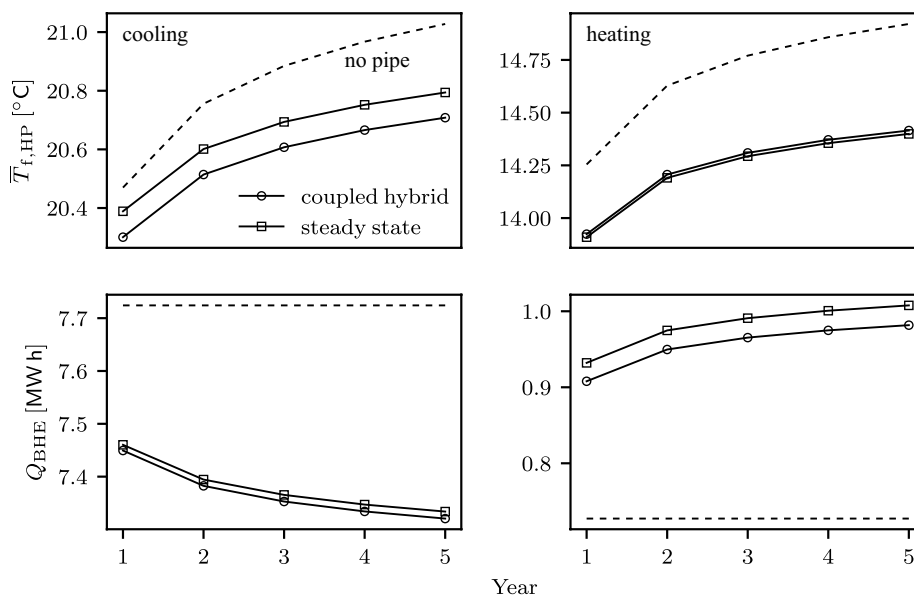
Fig. 20 Comparison between the proposed steady state approach and the coupled FLS ground and steady state pipe model for a 30 m connection pipe

for a 30m connection pipe. The differences are caused by the heat capacity of the borehole, which is not taken into account in the steady state model. For loads that are constant over a longer period of time, both models will converge as the steady-state assumption within the borehole underlying the borehole resistance approach becomes true. Figure 20 shows the analysis of average fluid temperatures and BHE load for the same scenario. The model is considered well suited for all scenarios where the influence of the borehole heat capacity is negligible.

Conclusions

In this study, three pipe models and three ground models were combined with each other to create connection pipe models for the investigation of heat losses in connection pipe networks in BHE installations. These were coupled with a BHE model and a highly simplified heat pump model. Scenarios with one and six pipe pairs with lengths of 30 and 60 m were simulated for a period of 5 years.

The steady-state pipe models with exponential and linear temperature profiles provide identical results for the investigated fluid temperatures and BHE loads. For the transient numerical pipe model, deviations occur for the short-term behaviour after control events of the heat pump. However, these have no effect on the overall assessment of BHE operation.

The numerical ground model with homogeneous properties and the FLS model provide almost identical results. The analysis of the temperature field in the ground has

shown that the dimensions of the numerical model were chosen too small, which, however, did not have a significant influence on the parameters investigated. The deviations between the two models mentioned and the numerical model with inhomogeneous properties depend on the actual properties. For the case chosen as an example here, however, it was shown that the differences between the two scenarios were rather small. The soil resistance model does not take into account temperature accumulation in the ground, nor the thermal interference of multiple pipes. This leads to significant deviations compared to the other models while overestimating the heat exchange along the connecting pipes.

Interestingly, during the simulation of six pairs of pipes in a shared trench and due to the bundled arrangement of the pipes and the thermal interference, the heat exchange per pipe with the surrounding ground decreased significantly. While the BHE heat load with one pair of 30 m pipes was increased by 40% due to the heat transfer along the connection pipes, it was always 10% for the case with six pairs of pipes. For the cooling loads, which are the dominant loads in the investigated scenario, the BHE load was reduced by 5% with one pair of pipes and only 2.6% with six pairs of pipes.

With regard to the computational effort, the steady-state linear model is the most efficient of all pipe models, followed by the steady state and the 1D numerical model. The FLS model required less computational time than the 2D numerical ground model, however this is only valid for the chosen model size and discretization. Furthermore, it should be noted that for the FLS model, due to the spatial and temporal superposition, the computational effort increases exponentially with increasing number of time steps as well as with increasing number of pipes.

The proposed steady-state model combines the findings from the previous comparison. By combining the well established borehole resistance approach for the BHE with a model of similar simplicity for the connection pipes, the model allows for an easy estimation of the load distribution between BHE and connection pipes for all cases in which the influence of the borehole heat capacity and short-time effects are negligible. The model can be simply extended to an arbitrary number of BHEs and connection pipes. For more complex pipe paths or inhomogeneous soil conditions, the pipe g-functions may need to be calculated numerically. However, once calculated they can be used within the proposed model for a variety of studies with different loads or thermal boundary conditions. In future work, we will use the model to investigate different climatic conditions.

Appendix

The results for all model combinations for one pair of connection pipes are listed in Table 7, results for six pairs of connection pipes are presented in Table 8.

Table 7 Compilation of all calculation results for the simulation of one pair of connection pipes

			1st year				2nd year				3rd year				4th year				5th year			
			T_c	T_h	Q_c	Q_h	T_c	T_h	Q_c	Q_h	T_c	T_h	Q_c	Q_h	T_c	T_h	Q_c	Q_h	T_c	T_h	Q_c	Q_h
No pipe			20.5	14.3	7.7	0.7	20.8	14.6	7.7	0.7	20.9	14.8	7.7	0.7	21.0	14.9	7.7	0.7	21.0	14.9	7.7	0.7
2Dnum hetero	1Dnum	30 m	20.3	14.0	7.47	0.84	20.5	14.3	7.42	0.88	20.6	14.4	7.39	0.89	20.7	14.5	7.38	0.9	20.7	14.6	7.37	0.9
		60 m	20.2	13.9	7.33	0.96	20.4	14.1	7.24	1.02	20.5	14.2	7.21	1.04	20.5	14.3	7.18	1.05	20.6	14.3	7.16	1.06
	Steady	30 m	20.3	14.0	7.47	0.84	20.5	14.3	7.42	0.87	20.6	14.4	7.39	0.89	20.7	14.5	7.38	0.9	20.8	14.6	7.37	0.9
		60 m	20.2	13.9	7.33	0.96	20.4	14.1	7.25	1.01	20.5	14.2	7.21	1.04	20.5	14.3	7.18	1.05	20.6	14.3	7.17	1.06
	SteadyLin	30 m	20.3	14.0	7.47	0.84	20.5	14.3	7.42	0.87	20.6	14.4	7.39	0.89	20.7	14.5	7.38	0.9	20.8	14.6	7.37	0.9
		60 m	20.2	13.9	7.33	0.96	20.4	14.1	7.25	1.02	20.5	14.2	7.21	1.04	20.5	14.3	7.18	1.05	20.6	14.3	7.17	1.06
2Dnum homo	1Dnum	30 m	20.3	13.9	7.45	0.91	20.5	14.2	7.38	0.95	20.6	14.3	7.35	0.97	20.7	14.4	7.33	0.98	20.7	14.4	7.32	0.98
		60 m	20.2	13.7	7.32	1.07	20.4	13.9	7.21	1.14	20.4	14.0	7.17	1.17	20.5	14.1	7.14	1.18	20.5	14.1	7.12	1.19
	Steady	30 m	20.3	13.9	7.45	0.91	20.5	14.2	7.38	0.95	20.6	14.3	7.35	0.96	20.7	14.4	7.33	0.97	20.7	14.4	7.32	0.98
		60 m	20.2	13.7	7.32	1.07	20.4	13.9	7.21	1.14	20.4	14.0	7.17	1.16	20.5	14.1	7.14	1.18	20.5	14.1	7.12	1.19
	SteadyLin	30 m	20.3	13.9	7.45	0.91	20.5	14.2	7.38	0.95	20.6	14.3	7.35	0.96	20.7	14.4	7.33	0.97	20.7	14.4	7.32	0.98
		60 m	20.2	13.7	7.31	1.07	20.4	13.9	7.21	1.14	20.4	14.0	7.17	1.16	20.5	14.1	7.14	1.18	20.5	14.1	7.12	1.19
FLS	1Dnum	30 m	20.3	13.9	7.45	0.91	20.5	14.2	7.38	0.95	20.6	14.3	7.35	0.97	20.7	14.4	7.33	0.98	20.7	14.4	7.32	0.98
		60 m	20.2	13.7	7.32	1.07	20.4	13.9	7.22	1.14	20.4	14.0	7.17	1.17	20.5	14.1	7.14	1.18	20.5	14.1	7.12	1.2
	Steady	30 m	20.3	13.9	7.45	0.91	20.5	14.2	7.38	0.95	20.6	14.3	7.35	0.97	20.7	14.4	7.33	0.97	20.7	14.4	7.32	0.98
		60 m	20.2	13.7	7.32	1.07	20.4	13.9	7.21	1.14	20.4	14.0	7.17	1.16	20.5	14.1	7.14	1.18	20.5	14.1	7.12	1.19
	SteadyLin	30 m	20.3	13.9	7.45	0.91	20.5	14.2	7.38	0.95	20.6	14.3	7.35	0.97	20.7	14.4	7.33	0.97	20.7	14.4	7.32	0.98
		60 m	20.2	13.7	7.32	1.07	20.4	13.9	7.21	1.14	20.4	14.0	7.17	1.16	20.5	14.1	7.14	1.18	20.5	14.1	7.12	1.19
R_{soil}	1Dnum	30 m	20.0	13.2	7.15	1.49	20.1	13.3	6.99	1.62	20.1	13.4	6.92	1.66	20.1	13.4	6.88	1.69	20.1	13.4	6.85	1.71
		60 m	19.9	12.9	7.03	1.73	20.0	13.0	6.84	1.88	20.0	13.0	6.77	1.93	20.0	13.0	6.72	1.96	20.0	13.1	6.69	1.98
	Steady	30 m	20.0	13.2	7.15	1.49	20.1	13.3	6.99	1.62	20.1	13.4	6.92	1.66	20.1	13.4	6.88	1.69	20.1	13.4	6.85	1.71
		60 m	19.9	12.9	7.03	1.73	20.0	13.0	6.84	1.88	20.0	13.0	6.77	1.93	20.0	13.0	6.72	1.96	20.0	13.1	6.69	1.98
	SteadyLin	30 m	20.0	13.2	7.15	1.49	20.1	13.3	6.99	1.62	20.1	13.4	6.92	1.66	20.1	13.4	6.88	1.69	20.1	13.4	6.85	1.71
		60 m	19.9	12.9	7.03	1.73	20.0	13.0	6.84	1.88	20.0	13.0	6.76	1.93	20.0	13.0	6.72	1.96	20.0	13.1	6.69	1.98

Table 8 Compilation of all calculation results for the simulation of six pairs of connection pipes

			1st year				2nd year				3rd year				4th year				5th year			
			T_c	T_h	Q_c	Q_h	T_c	T_h	Q_c	Q_h	T_c	T_h	Q_c	Q_h	T_c	T_h	Q_c	Q_h	T_c	T_h	Q_c	Q_h
No pipe			20.5	14.3	7.7	0.7	20.8	14.6	7.7	0.7	20.9	14.8	7.7	0.7	21.0	14.9	7.7	0.7	21.0	14.9	7.7	0.7
2Dnum hetero	1Dnum	30 m	20.4	14.2	7.55	0.73	20.6	14.6	7.53	0.74	20.8	14.7	7.51	0.75	20.8	14.8	7.51	0.75	20.9	14.8	7.5	0.75
		60 m	20.3	14.2	7.43	0.76	20.6	14.5	7.39	0.78	20.7	14.6	7.37	0.79	20.7	14.7	7.36	0.8	20.8	14.7	7.35	0.8
	Steady	30 m	20.4	14.2	7.55	0.73	20.6	14.6	7.53	0.74	20.8	14.7	7.51	0.75	20.8	14.8	7.51	0.75	20.9	14.8	7.5	0.75
		60 m	20.3	14.2	7.43	0.76	20.6	14.5	7.39	0.78	20.7	14.6	7.37	0.79	20.7	14.7	7.36	0.8	20.8	14.7	7.35	0.8
	SteadyLin	30 m	20.4	14.2	7.55	0.73	20.6	14.6	7.53	0.74	20.8	14.7	7.51	0.75	20.8	14.8	7.51	0.75	20.9	14.8	7.5	0.75
		60 m	20.3	14.2	7.43	0.76	20.6	14.5	7.39	0.78	20.7	14.6	7.37	0.79	20.7	14.7	7.36	0.8	20.8	14.7	7.35	0.8
2Dnum homo	1Dnum	30 m	20.4	14.2	7.54	0.74	20.6	14.5	7.52	0.76	20.8	14.7	7.5	0.76	20.8	14.7	7.5	0.77	20.9	14.8	7.49	0.77
		60 m	20.3	14.1	7.43	0.78	20.6	14.4	7.38	0.81	20.7	14.6	7.35	0.82	20.7	14.6	7.34	0.83	20.8	14.7	7.33	0.83
	Steady	30 m	20.4	14.2	7.54	0.74	20.6	14.5	7.52	0.76	20.8	14.7	7.5	0.76	20.8	14.7	7.5	0.77	20.9	14.8	7.49	0.77
		60 m	20.3	14.1	7.43	0.78	20.6	14.4	7.38	0.81	20.7	14.6	7.35	0.82	20.7	14.6	7.34	0.83	20.8	14.7	7.33	0.83
	SteadyLin	30 m	20.4	14.2	7.54	0.74	20.6	14.5	7.52	0.76	20.8	14.7	7.5	0.76	20.8	14.7	7.5	0.77	20.9	14.8	7.49	0.77
		60 m	20.3	14.1	7.42	0.78	20.6	14.4	7.38	0.81	20.7	14.6	7.35	0.82	20.7	14.6	7.34	0.83	20.8	14.7	7.33	0.83
FLS	1Dnum	30 m	20.4	14.2	7.54	0.74	20.6	14.5	7.52	0.76	20.8	14.7	7.51	0.76	20.8	14.7	7.5	0.77	20.9	14.8	7.49	0.77
		60 m	20.3	14.1	7.43	0.79	20.6	14.4	7.38	0.81	20.7	14.6	7.36	0.82	20.7	14.6	7.34	0.83	20.8	14.7	7.33	0.84
	Steady	30 m	20.4	14.2	7.54	0.75	20.6	14.5	7.52	0.76	20.8	14.6	7.5	0.77	20.8	14.7	7.5	0.77	20.9	14.8	7.49	0.77
		60 m	20.3	14.1	7.43	0.79	20.6	14.4	7.38	0.81	20.7	14.5	7.36	0.83	20.7	14.6	7.34	0.83	20.8	14.7	7.33	0.84
	SteadyLin	30 m	20.4	14.2	7.54	0.75	20.6	14.5	7.52	0.76	20.8	14.6	7.5	0.77	20.8	14.7	7.5	0.77	20.9	14.8	7.49	0.77
		60 m	20.3	14.1	7.43	0.79	20.6	14.4	7.38	0.81	20.7	14.5	7.36	0.83	20.7	14.6	7.34	0.83	20.8	14.7	7.33	0.84
R_{soil}	1Dnum	30 m	20.0	13.3	7.12	1.46	20.1	13.4	6.96	1.59	20.1	13.4	6.89	1.63	20.1	13.4	6.85	1.66	20.1	13.5	6.82	1.68
		60 m	19.9	13.0	7.0	1.7	19.9	13.1	6.82	1.85	20.0	13.1	6.74	1.9	20.0	13.1	6.69	1.93	20.0	13.1	6.66	1.95
	Steady	30 m	20.0	13.7	7.11	1.17	20.1	13.4	6.95	1.59	20.1	13.4	6.89	1.63	20.1	13.4	6.85	1.66	20.1	13.5	6.82	1.68
		60 m	19.9	13.0	7.0	1.7	19.9	13.1	6.81	1.85	20.0	13.1	6.74	1.9	20.0	13.1	6.69	1.93	20.0	13.1	6.66	1.95
	SteadyLin	30 m	20.0	13.3	7.12	1.46	20.1	13.4	6.96	1.59	20.1	13.4	6.89	1.63	20.1	13.4	6.85	1.66	20.1	13.5	6.82	1.68
		60 m	19.9	13.0	7.0	1.7	19.9	13.1	6.81	1.85	20.0	13.1	6.74	1.9	20.0	13.1	6.69	1.93	20.0	13.1	6.66	1.95

Abbreviations

Latin symbols

A_i	Inner cross-sectional area of pipe
c	Specific heat capacity
$d_{p,i}$	Pipe inner diameter
g	G-function
H	Length of line source
l	Length
Nu	Nusselt number
Pr	Prandtl number
q	Length-related thermal load
q_v	Source term
Q_{tot}	Total load
r	Radial distance
$r_{p,i}$	Pipe inner radius
$r_{p,o}$	Pipe outer radius
R_{conv}	Convective thermal resistance
R_{fs}	Fluid-to-soil thermal resistance
R_p	Pipe thermal resistance
Re	Reynolds number
s	Variable of integration
t	Time
T	Temperature
T_0	Undisturbed ground temperature
u	Velocity
V	Fluid volumetric flow rate
x, y, z	Spatial coordinates

Greek symbols

α	Thermal diffusivity
η	Dynamic viscosity
λ	Thermal conductivity
ρ	Density
Φ	Specific heat transfer coefficient

Subscripts

b	Borehole
f	Fluid
in	Inlet
out	Outlet
p	Pipe
s	Soil

Abbreviations

BHE	Borehole heat exchanger
HP	Heat pump
FLS	Finite line source

Author contributions
SD has done the conceptualization, methodology, formal analysis, investigation, writing of the original draft and visualization. RF and GAN are responsible for review and editing as well as supervision. All authors read and approved the final manuscript.

Availability of data and materials
Data available on request.

Declaration

References

Ahmadfard M, Bernier M. A review of vertical ground heat exchanger sizing tools including an inter-model comparison. Renew & Sustain Energy Rev. 2019;110:247–65. https://doi.org/10.1016/j.rser.2019.04.045.

Bauer D, Heidemann W, Müller-Steinhagen H, Diersch H-JG. Thermal resistance and capacity models for borehole heat exchangers. Int J Energy Res. 2011;35(4):312–20. https://doi.org/10.1002/er.1689.

Bortoloni M, Bottarelli M, Su YH. A study on the effect of ground surface boundary conditions in modelling shallow ground heat exchangers. Appl Thermal Eng. 2017;111:1371–7. https://doi.org/10.1016/j.applthermaleng.2016.05.063.

Carslaw HS, Jaeger JC. Conduction of heat in solids. Oxford: Oxford University; 1959.

Chen S, Witte F, Kolditz O, Shao HB. Shifted thermal extraction rates in large borehole heat exchanger array - a numerical experiment. Appl Thermal Eng. 2020. https://doi.org/10.1016/j.applthermaleng.2019.114750.

Chen S, Cai WL, Witte F, Wang XR, Wang FH, Kolditz O, Shao HB. Long-term thermal imbalance in large borehole heat exchangers array - a numerical study based on the leicester project. Energy Build. 2021. https://doi.org/10.1016/j.enbuild.2020.110518.

Chung M, Jung PS, Rangel RH. Semi-analytical solution for heat transfer from a buried pipe with convection on the exposed surface. Int J Heat Mass Tran. 1999;42(20):3771–86. https://doi.org/10.1016/S0017-9310(99)00046-0.

Claesson J, Dunand A. Heat extraction from the ground by horizontal pipes: a mathematical analysis. Lund: Lund University; 1983.

Claesson J, Javed S. An analytical method to calculate borehole fluid temperatures for time-scales from minutes to decades. ASHRAE Transact. 2011;117:279–88.

Cui YL, Zhu J, Twaha S, Chu JZ, Bai HY, Huang K, Chen XJ, Zoras S, Soleimani Z. Techno-economic assessment of the horizontal geothermal heat pump systems: a comprehensive review. Energy Convers Manag. 2019;191:208–36. https://doi.org/10.1016/j.enconman.2019.04.018.

Dasare RR, Saha SK. Numerical study of horizontal ground heat exchanger for high energy demand applications. Appl Thermal Eng. 2015;85:252–63. https://doi.org/10.1016/j.applthermaleng.2015.04.014.

Düber S, Ziegler M, Fuentes R. Development and validation of a computationally efficient hybrid model for temporal high-resolution simulations of geothermal bore fields. Int J Numerical Analytical Methods Geomechanics. 2022. https://doi.org/10.1002/nag.3427.

Energietechnik V-F. Thermal use of the underground - ground source heat pump systems. VDI-Gesellschaft Energie und Umwelt. 2019.

Eskilson P. Thermal analysis of heat extraction boreholes [ph. d. thesis]. Lund: University of Lund. 1987.

Fontaine PO, Marcotte D, Pasquier P, Thibodeau D. Modeling of horizontal geoexchange systems for building heating and permafrost stabilization. Geothermics. 2011;40(3):211–20. https://doi.org/10.1016/j.geothermics.2011.07.002.

Gan GH. A numerical methodology for comprehensive assessment of the dynamic thermal performance of horizontal ground heat exchangers. Thermal Sci Eng Progress. 2019;11:365–79. https://doi.org/10.1016/j.tsep.2019.04.013.

Gnielinski V. G1 Durchströmte Rohre. Berlin, Heidelberg: Springer; 2013.

Gu X, Makasis N, Motamedi Y, Narsilio GA, Arulrajah A, Horpibulsuk S. Geothermal pavements: field observations, numerical modelling and long-term performance. Géotechnique. 2022;72(9):832–46. https://doi.org/10.1680/jgeot.20.P.296.

Hastaoglu MA, Negiz A, Heidemann R. Three-dimensional transient heat transfer from a buried pipe part iii comprehensive model. Chem Eng Sci. 1995;50(16):2545–55.

Himasekhar K, Bau HH. Thermal convection associated with hot/cold pipes buried in a semi-infinite, saturated, porous medium. Int J Heat Mass Trans. 1987;30(2):263–73.

Hou G, Taherian H, Song Y, Jiang W, Chen DA. systematic review on optimal analysis of horizontal heat exchangers in ground source heat pump systems. Renew Sustain Energy Rev. 2022. https://doi.org/10.1016/j.rser.2021.111830.

Ioffe I. A problem of transient heat conduction in a semibounded body with an internal cylindrical heat source. J Eng Phys. 1972;23(2):1051–4.

Javed S, Spitler JD. Calculation of borehole thermal resistance. 2016. 10.1016/b978-0-08-100311-4.00003-0

Kavanaugh SP, Rafferty KD. Geothermal heating and cooling: design of ground-source heat pump systems. Peachtree Corners: ASHRAE; 2014.

Kayaci N, Demir H. Numerical modelling of transient soil temperature distribution for horizontal ground heat exchanger of ground source heat pump. Geothermics. 2018;73:33–47. https://doi.org/10.1016/j.geothermics.2018.01.009.

Lamarche L. Analytical g-function for inclined boreholes in ground-source heat pump systems. Geothermics. 2011;40(4):241–9. https://doi.org/10.1016/j.geothermics.2011.07.006.

Lamarche L. Horizontal ground heat exchangers modelling. Appl Thermal Eng. 2019;155:534–45. https://doi.org/10.1016/j.applthermaleng.2019.04.006.

Larwa B, Kupiec K. Heat transfer in the ground with a horizontal heat exchanger installed - long-term thermal effects. Appl Thermal Eng. 2020. https://doi.org/10.1016/j.applthermaleng.2019.114539.

Li H, Nagano K, Lai YX. A new model and solutions for a spiral heat exchanger and its experimental validation. Int J Heat Mass Trans. 2012;55(15–16):4404–14. https://doi.org/10.1016/j.ijheatmasstransfer.2012.03.084.

Düber *et al. Geothermal Energy*   (2023) 11:15

Page 32 of 32

Li M, Li P, Chan V, Lai ACK. Full-scale temperature response function (g-function) for heat transfer by borehole ground heat exchangers (ghes) from sub-hour to decades. Appl Energy. 2014;136:197–205. https://doi.org/10.1016/j.apenergy.2014.09.013.

Lund JW, Toth AN. Direct utilization of geothermal energy 2020 worldwide review. Geothermics. 2021. https://doi.org/10.1016/j.geothermics.2020.101915.

Luo J, Rohn J, Bayer M, Priess A. Modeling and experiments on energy loss in horizontal connecting pipe of vertical ground source heat pump system. Appl Thermal Eng. 2013;61(2):55–64. https://doi.org/10.1016/j.applthermaleng.2013.07.022.

Marcotte D, Pasquier P. Fast fluid and ground temperature computation for geothermal ground-loop heat exchanger systems. Geothermics. 2008;37(6):651–65.

Martin W, Sadhal S. Bounds on transient temperature distribution due to a buried cylindrical heat source. Int J Heat Mass Trans. 1978;21(6):783–9.

Muñoz-Criollo JJ, Cleall PJ, Rees SW. Factors influencing collection performance of near surface interseasonal ground energy collection and storage systems. Geomechanics Energy Environ. 2016;6:45–57. https://doi.org/10.1016/j.gete.2016.04.001.

Piechowski M. Heat and mass transfer model of a ground heat exchanger: theoretical development. Int J Energy Res. 1999;23(7):571–88.

Selamat S, Miyara A, Kariya K. Numerical study of horizontal ground heat exchangers for design optimization. Renew Energy. 2016;95:561–73. https://doi.org/10.1016/j.renene.2016.04.042.

Shafagh I, Shepley P, Shepherd W, Loveridge F, Schellart A, Tait S, Rees SJ. Thermal energy transfer around buried pipe infrastructure. Geomechanics Energy Environ. 2022. https://doi.org/10.1016/j.gete.2021.100273.

Thiyagarajan R, Yovanovich MM. Thermal resistance of a buried cylinder with constant flux boundary condition. J Heat Trans. 1974;96(2):249–50. https://doi.org/10.1115/1.3450174.

Tian X, Mao R, Pei P, Wu H, Ma H, Hu C, Zhang Z. Experimental study on temperature control optimization of ground source heat pump horizontal headers. Energy Build. 2022. https://doi.org/10.1016/j.enbuild.2022.112541.

Urresta E, Moya M, Campana C, Cruz C. Ground thermal conductivity estimation using the thermal response test with a horizontal ground heat exchanger. Geothermics. 2021. https://doi.org/10.1016/j.geothermics.2021.102213.

Van Genuchten MT. Analytical Solutions of the One-dimensional Convective-dispersive Solute Transport Equation, vol. 1661. Maryland: US Department of Agriculture Agricultural Research Agricultural Research Service: US Department of Agricultural Research Service; 1982.

Wetter M, Huber A. Vertical borehole heat exchanger ews model. TRNSYS type. 1997.

Wu YP, Gan GH, Verhoef A, Vidale PL, Gonzalez RG. Experimental measurement and numerical simulation of horizontal-coupled slinky ground source heat exchangers. Appl Thermal Eng. 2010;30(16):2574–83. https://doi.org/10.1016/j.applthermaleng.2010.07.008.

Xiong ZY, Fisher DE, Spitler JD. Development and validation of a slinky(tm) ground heat exchanger model. Appl Energy. 2015;141:57–69. https://doi.org/10.1016/j.apenergy.2014.11.058.

Zhang MF, Gong GC, Zeng LW. Investigation for a novel optimization design method of ground source heat pump based on hydraulic characteristics of buried pipe network. Appl Thermal Eng. 2021. https://doi.org/10.1016/j.applthermaleng.2020.116069.

Publisher's Note